10-15-2020

Drainage evolution and exhumation history of the eastern Himalaya: Insights from the Nicobar Fan, northeastern Indian Ocean

Wen Huang Chen
Guangzhou Institute of Geochemistry Chinese Academy of Sciences

Yi Yan
Guangzhou Institute of Geochemistry Chinese Academy of Sciences

Peter D. Clift
Louisiana State University

Andrew Carter
Birkbeck, University of London

Chi Yue Huang
Tongji University

See next page for additional authors

Recommended Citation

Chen, W., Yan, Y., Clift, P., Carter, A., Huang, C., Pickering, K., Chemale, F., Shan, Y., & Zhang, X. (2020). Drainage evolution and exhumation history of the eastern Himalaya: Insights from the Nicobar Fan, northeastern Indian Ocean. *Earth and Planetary Science Letters, 548* https://doi.org/10.1016/j.epsl.2020.116472

Drainage evolution and exhumation history of the eastern Himalaya: Insights from the Nicobar Fan, northeastern Indian Ocean

Wen-Huang Chen[1, 2, 3*], Yi Yan[1*], Peter D. Clift[4], Andrew Carter[5], Chi-Yue Huang[6], Kevin T. Pickering[7], Farid Chemale Jr.[8], Yehua Shan[1], and Xinchang Zhang[1]

[1]Key Laboratory of Ocean and Marginal Sea Geology, Guangzhou Institute of Geochemistry, Chinese Academy of Sciences, Guangzhou 510640, China

[2]Southern Marine Science and Engineering Guangdong Laboratory (Guangzhou), Guangzhou 511458, China

[3]Innovation Academy of South China Sea Ecology and Environmental Engineering, Chinese Academy of Sciences, Guangzhou, 510640, China

[4]Department of Geology and Geophysics, Louisiana State University, Baton Rouge, LA 70803, USA

[5]Department of Earth and Planetary Sciences, Birkbeck, University of London, Malet Street, London WC1E 7HX, United Kingdom

[6]School of Ocean and Earth Science, Tongji University, Shanghai 200092, China

[7]Department of Earth Sciences, University College London (UCL), London WC1E 6BT, United Kingdom

[8]Programa de Pós-Graduação em Geologia, Universidade do Vale do Rio dos Sinos, 93.022-750 São Leopoldo, RS, Brazil

*Corresponding Authors: Wen-Huang Chen, chenwenhuang@gig.ac.cn, and Yi Yan, yanyi@gig.ac.cn

Abstract

The eastern Himalayan syntaxis, where the Yarlung Tsangpo sharply bends, is one of the areas experiencing most rapid exhumation on Earth. The rapid exhumation is often regarded as the result of capture of the Yarlung Tsangpo by the Brahmaputra River. However, both the timing of integration of the Yarlung Tsangpo-Brahmaputra River and initiation of the rapid syntaxial exhumation are debated. As the ultimate sedimentary trap of the Yarlung Tsangpo-Brahmaputra River, the Nicobar Fan is a window to look into the drainage evolution and exhumation history of the eastern Himalaya. International Ocean Discovery Program Expedition 362 drilled the Nicobar Fan for the first time, recovering fan sediments dating back to the Early Miocene (~19 Ma). We apply trace elements and Sr-Nd isotopes to investigate the provenance of the sediments in the Nicobar Fan with the aim of constraining the timing of integration of the Yarlung Tsangpo-Brahmaputra River and initiation of the rapid syntaxial exhumation. The geochemical and Sr-Nd isotope compositions indicate an eastern Himalayan source dominated by the Greater Himalaya, with significant Gangdese arc contribution and primarily carried by the Brahmaputra River. Flux of Gangdese arc material appears to have been continuous from the base of the Nicobar Fan, suggesting that the Yarlung Tsangpo-Brahmaputra River has been established at least since ~19 Ma. Synchronously with the sharp rise in sedimentation rate, the abrupt change of geochemical and isotope compositions at ~9.2 Ma indicates an increase in erosion of the Greater Himalaya as the result of initiation of rapid exhumation

in the broad syntaxial region. The proportion of Greater Himalayan material increased again at 3.5–1.7 Ma, consistent with a younger pulse of rapid exhumation focused in the core of the syntaxis since ~3.5 Ma. Our results show that initiation of the rapid syntaxial exhumation postdated integration of the Yarlung Tsangpo-Brahmaputra River by at least ~10 m.y. Therefore, tectonic uplift rather than river capture could be responsible for the initiation of the rapid syntaxial exhumation.

Key words: Nicobar Fan, Yarlung Tsangpo-Brahmaputra River, eastern Himalayan syntaxis, sedimentary record, International Ocean Discovery Program Expedition 362

1. Introduction

Collisional tectonics induces topographic variation and results in drainage reorganization via mechanisms such as river capture, diversion and reversal (e.g. Brookfield, 1998; Clark et al., 2004). Drainage reorganization markedly affects the distribution and intensity of erosion over an orogen, which in turn influences the style and location of crustal deformation (Cina et al., 2009). Therefore, study of drainage evolution during collisional orogeny is crucial to understanding the complex interplay between tectonic deformation and surface erosion (e.g. Bracciali et al., 2015). The Himalayan orogen, where active collision is ongoing and major South Asian rivers originate, is an ideal place in which to recognize tectonic-erosion interactions. The eastern Himalayan syntaxis is one of the most active tectonic regions on Earth and characterized by very rapid rock uplift and exhumation (Burg et al., 1997; Ding et al., 2001) (Fig. 1). The Yarlung Tsangpo runs eastward along the suture between the Himalaya and the Lhasa block, and then sharply bends southward through the eastern

66 syntaxis, carving one of the world's largest and deepest gorges, the Yarlung Tsangpo
67 Gorge. Downstream of the gorge, the Yarlung Tsangpo is called the Siang River and
68 becomes the southwestward-flowing Brahmaputra River in the Himalayan foreland. It
69 then meets the Ganges River, and finally discharges into the Bay of Bengal and the
70 northeastern Indian Ocean, where it accumulates as the Bengal-Nicobar Fan system (Fig.
71 1). The sediments are now transferred to the Bengal Fan by turbidite currents via the
72 Swatch-of-No-Ground submarine canyon and the Active Channel (Fig. 1) which has been
73 active since 12.5 ka BP, however, there were probably more than one canyon-channel
74 system at times before then (Curray et al., 2003). The Bengal-Nicobar Fan system
75 extends southward for over 3000 km to ~7°S and covers an area of ~4×10^6 km^2 with a
76 volume of >8×10^6 km^3 since ca. 20 Ma (Curray et al., 2003, Pickering et al., 2020). As
77 the ultimate sediment trap of the Ganges River and Yarlung Tsangpo-Brahmaputra River,
78 the Bengal-Nicobar Fan preserves records of Himalayan erosion and is therefore vital to
79 deciphering the drainage evolution and exhumation history of the eastern Himalaya.

80 The eastern Himalayan syntaxis presently feeds 45–70% of the bulk sediment flux
81 of the Brahmaputra River, suggesting an exhumation rate up to 10 mm/yr or more (e.g.
82 Singh and France-Lanord, 2002; Bracciali et al., 2016). Such high exhumation rates are
83 also supported by the bedrock cooling age as young as <1 Ma (e.g. Seward and Burg,
84 2008). To explain the extremely rapid syntaxial exhumation, most researchers emphasize
85 the role of tectonics caused by northward indentation of the northeastern corner of the
86 Indian plate into Eurasia, which leads to growth of the syntaxis (e.g. Burg et al., 1997;
87 Seward and Burg, 2008; Bendick and Ehlers, 2014). However, the "tectonic aneurysm"
88 model highlights the potential coupling between tectonics and erosion and associates the

89 rapid exhumation with the incision of the Yarlung Tsangpo Gorge (Zeitler et al., 2001,
90 2014). This model suggests that rapid, focused erosion weakens the upper crust, leading
91 to lower crustal flow into the weakened zone, and promoting the doming of the upper
92 crust, thus generating a self-sustaining feedback between tectonic deformation and
93 surface erosion (Zeitler et al., 2001). This model also suggests that initiation of the rapid
94 syntaxial exhumation could be triggered by capture of the Yarlung Tsangpo by the
95 Brahmaputra River (Zeitler et al., 2001). However, both the timing of integration of the
96 Yarlung Tsangpo-Brahmaputra River and initiation of the rapid syntaxial exhumation
97 continue to be debated (e.g. Bracciali et al. 2015, 2016; Najman et al., 2019).

98 It has been proposed that the Yarlung Tsangpo flowed southeastward into the
99 Irrawaddy River through the Parlung Tsangpo, before it was captured by the Siang-
100 Brahmaputra River at ~10 Ma (Brookfield, 1998) or 3–4 Ma (Zeitler et al., 2001; Clark et
101 al., 2004). The timing of this capture event was however estimated based on the proposed
102 age of the localized uplift of the eastern syntaxis. Recent provenance analyses of the
103 paleo-Brahmaputra deposits provide new time constraints on integration of the Yarlung
104 Tsangpo-Brahmaputra River, to be either in the Late Miocene or the Early Miocene. The
105 first appearance of Gangdese arc detritus, indicative of a Yarlung Tsangpo contribution,
106 in the eastern Himalayan foreland basin were detected at ~10 Ma (Cina et al., 2009), at
107 ~7 Ma (Chirouze et al., 2013) and in the Early Miocene (Lang and Huntington, 2014) in
108 various sections. Meanwhile, Bracciali et al. (2015) observed the first influx of Gangdese
109 arc material in Lower Miocene sediments of the Surma Basin (northeastern Bengal Basin)
110 downstream of the Brahmaputra River. The timing of onset of the rapid syntaxial
111 exhumation remains poorly constrained, varying from the Late Miocene to the Plio-

112 Pleistocene (11–2 Ma). Most of the bedrock thermochronology data from the syntaxial
113 region show young cooling ages and indicate onset of rapid exhumation since ~3.5 Ma
114 (e.g. Burg et al., 1997; Seward and Burg, 2008). However, bedrock zircon U-Pb
115 geochronology denoted local melting accompanying rapid cooling since ~11–9.7 Ma
116 (Ding et al., 2001; Booth et al., 2004). A synthesis study of cooling history within and
117 around the syntaxis indicates a significant pulse of rapid exhumation at 10–5 Ma (Zeitler
118 et al., 2014). The paleo-Brahmaputra detrital records could offer a long-term exhumation
119 history of the syntaxis after the integration of the Yarlung Tsangpo-Brahmaputra River,
120 which avoids problems associated with study of the syntaxis bedrock where erosion and
121 metamorphism have removed or obscured the early exhumation history. However,
122 estimates of the onset of rapid exhumation interpreted from detrital thermochronology are
123 also variable. Rapid exhumation was recorded in the eastern Himalayan foreland basin by
124 7–5 Ma (Lang et al., 2016), in the Surma Basin since ~3.5–2 Ma (Bracciali et al. 2016)
125 and in the Bengal Fan since ~3.5 Ma (Najman et al., 2019), as indicated by the first
126 occurrence of detrital minerals with short lag times.

127 International Ocean Discovery Program (IODP) Expedition 362 successfully cored
128 Nicobar Fan sediments dating back to the Early Miocene (~19 Ma) (Fig. 1). These
129 sediments represent a key sedimentary archive of eastern Himalayan evolution (McNeill
130 et al., 2017a, 2017b). The Nicobar Fan sediments was transported for a long distance over
131 1700 km from the outlet. Therefore, compared to the proximal records of the fluvial-
132 deltaic Himalayan foreland basin and Surma Basin, the Nicobar Fan sediments might be
133 expected to minimize local effects that would obscure the upstream signal, and also
134 provide a continuous marine sedimentary succession with better depositional age

constraints. Evidence from the Bengal Basin and the Bay of Bengal indicates that the Ganges River and the Brahmaputra River entered the Bay of Bengal separately at some time in the past (e.g. Curray et al. 2003; Govin et al., 2018), rather than merging together before entering the bay as they do today. Therefore, compared to the Bengal Fan, the Nicobar Fan in the east should be less influenced by the signal of the Ganges River that drains the central Himalaya and peninsular India. Any significant contribution from the Irrawaddy River to the Nicobar Fan is unlikely as it requires transfer of the sediments across the forearc to the west, which was restricted by the then exposed Yadana-M8 Highs and the uplifted Sewell-Alcock Rises west of the Andaman Sea (Racey and Ridd, 2015) (Fig. 1). Sediment isopaches of the Cenozoic Martaban basin in the Andaman Sea related to the development of the Salween-Irrawaddy delta also show no significant sediment transfer to the west (Racey and Ridd, 2015) (Fig. 1). Because the Himalayan units and the Gangdese arc have contrasting lithologies and geochemistry (e.g. Singh et al., 2008; Wu et al., 2010) (Table 1), we conduct a provenance analysis of the Nicobar Fan sediments using trace elements and Sr-Nd isotope composition. Specifically, we aim to constrain the timing of integration of the Yarlung Tsangpo-Brahmaputra River by detecting the first appearance of Gangdese arc material, and attempt to estimate the timing of initiation of rapid exhumation of the eastern Himalayan syntaxis from the perspective of a provenance shift. Lastly, we evaluate the interaction between the rapid syntaxial exhumation and the Yarlung Tsangpo-Brahmaputra River evolution.

2. Background

2.1.Tectonic setting of the eastern Himalaya

158 The collision between the Indian and Eurasian plates, beginning at 65–43 Ma,
159 deformed and uplifted the northern margin of the Indian continent to form the Himalayan
160 orogen (Yin, 2006). The Himalaya is separated from the Lhasa block of the Eurasian
161 plate by the Indus-Yarlung Suture Zone (Fig. 1). The southern Lhasa block is intruded by
162 Cretaceous–Paleogene magmatic and volcanic rocks of the Andean-type Gangdese arc,
163 resulting from the northward subduction of the Tethyan Ocean (e.g. Copeland et al.,
164 1995). South of the suture, the Himalaya is classically divided into four lithotectonic
165 units: the Tethyan Himalaya (Paleoproterozoic–Eocene sedimentary cover), the Greater
166 Himalaya (medium- to high-grade Paleoproterozoic–Ordovician metamorphic crystalline
167 rocks), the Lesser Himalaya (Proterozoic–Cambrian metasedimentary and sedimentary
168 rocks) and the Sub-Himalaya (Cenozoic foreland basin sediments) (Yin, 2006) (Fig. 1).
169 Rapid exhumation of the Greater Himalaya at the rate of 2–5 mm/yr initiated at ~23 Ma,
170 associated with movement on the Main Central Thrust and the South Tibetan Detachment
171 System (Fig. 1), and ceased around 18–16 Ma in the western and central Himalaya and
172 around 14–10 Ma in the eastern Himalaya (Najman et al., 2019 and references therein).
173 The Gangdese arc shows significantly higher ε_{Nd} and lower $^{87}Sr/^{86}Sr$ than the Himalayan
174 units, while the Lesser Himalaya have the lowest ε_{Nd} and most radiogenic $^{87}Sr/^{86}Sr$
175 among the Himalayan units (Singh et al., 2008; Wu et al., 2010) (Table 1).

176 The eastern Himalayan syntaxis is mainly composed of high-grade metamorphic
177 crystalline rocks of the Greater Himalaya, which forms the peak of Namche Barwa (7782
178 m) in the core of the syntaxis (Ding et al., 2001). The syntaxis is a north-plunging
179 antiformal and in part domal structure (Bracciali et al., 2016). The Greater Himalaya in
180 the syntaxis shared a similar tectonothermal history with that in the main belt of the

Himalaya before their evolution diverged in the Late Miocene (Najman et al., 2019). Thereafter, the Greater Himalaya showed younger metamorphism and more rapid exhumation (up to 10 mm/yr or more) in the syntaxis. Along the sharply curved eastern Himalayan syntaxis, the WNW-ESE trending Himalayan collisional belt passes abruptly into the N-S striking Indo-Burman Ranges (Fig. 1). The Indo-Burman Ranges is divided laterally into two portions. The Neogene Indo-Burman Ranges in the west represent Himalayan-derived Bengal-Nicobar Fan sediments incorporated into the accretionary prism, whereas the Paleogene Indo-Burman Ranges in the east were interpreted as forearc sediments equivalent to the Central Myanmar Basin or trench sediments with significant input from the Burmese arc (including the Wuntho-Popa Arc and the Cretaceous–Paleogene plutons intruding the Mogok Metamorphic Belt) (Allen et al., 2008). The Burmese arc overall shows similar Sr-Nd isotope compositions to the Gangdese arc (Wu et al., 2010; Lin et al., 2019) (Table 1).

2.2.Litho-stratigraphy and age model of the Nicobar Fan

The Nicobar Fan is separated from the Bengal Fan by the Ninetyeast Ridge (formed from 77 to 43 Ma, Frey et al., 2015) and now being subducted beneath the Sumatra margin. IODP Expedition 362 drilled two sites on the northern Nicobar Fan east of the Ninetyeast Ridge in 2016, recovering the complete sedimentary succession at Site U1480 to a basement depth of 1415.53 meter below seafloor (mbsf), and from 1149.7 mbsf to within 10s m of basement at 1500 mbsf at Site U1481 (McNeil et al., 2017a) (Figs. 1 and 2). At Site U1480, Units I–IIIA (0–1310.02 mbsf) represent the Nicobar Fan and are composed predominantly of siliciclastic sediment gravity-flow deposits (mostly

204 turbidities) like the Bengal Fan (McNeil et al., 2017a). Unit I is 26.42 m-thick, and
205 contains calcareous mud and interbeds of fine sand and mud. Unit II (1223.93 m-thick) is
206 characterized by frequent occurrence of fine sand and sandy silt alternating with mud and
207 is divided into three subunits. Unit IIIA is only 59.67 m-thick and contains gray-green
208 and minor reddish-brown mudstone with rare thin-bedded siltstone, representing the
209 earliest depositional phase of the fan. At Site U1481, the upper ~210 m of the
210 sedimentary succession is equivalent to Unit IIC at Site U1480, while the lower ~140 m
211 corresponds to Unit IIIA but includes a ~20 m-thick bed of fine-grained sandstone and
212 siltstone at its base (McNeil et al., 2017a).

213 The shipboard age models of Expedition 362 sites were generated using microfossils
214 (McNeil et al., 2017a). Backman et al. (2019) later proposed a revised age model of Site
215 U1480 taking post-cruise biostratigraphic data into account. According to the above age
216 models, the base of the Nicobar Fan at Site U1480 (1250.35 mbsf) is estimated at ~15.3
217 Ma, however, the lowest Nicobar Fan sediments (1500 mbsf) at Site U1481 is estimated
218 older at ~19.2 Ma (Fig. 2). Thicker Unit IIIA at Site U1481 with older and coarser
219 siliciclastic sediments potentially reflects topographic variations, because the site is less
220 proximal to the Ninetyeast Ridge and has deeper basement. At both sites, sedimentation
221 rates increased dramatically and synchronously at ~9.2 Ma corresponding to the Units
222 IIIA and IIC boundary (Fig. 2), from 8–15 m/m.y. to ~220 m/m.y. (Fig. 5). This timing
223 was placed at ~9.5 Ma by McNeil et al. (2017b), but it should be ~9.2 Ma according to
224 the age models of McNeil (2017a) and Backman et al. (2019). At Site U1480, the high
225 sedimentation rate persisted, but decreased slightly to 65–125 m/m.y. at 5.9 Ma and
226 subsequently increased to 290 m/m.y. at ~2.4 Ma (Fig. 5). The sedimentation rate then

227 dropped to 3–42 m/m.y. since ~1.7 Ma (Units I and II boundary), which was interpreted
228 as fan abandonment due to tectonic blocking of the sediment routing to the Nicobar Fan
229 by the Ninetyeast Ridge as it collided with the Sunda margin (McNeil et al., 2017a).

230

231 ## 3. Methods

232 We conducted trace element and Sr-Nd isotopic analyses on the bulk silicate fraction
233 of the Nicobar Fan muds/mudstones, in an attempt to trace provenance variations. A total
234 of sixty-eight core samples were collected (Fig. 2), primarily from the mud/mudstone of
235 the upper part of turbidite beds. The samples were leached with 2N acetic acid to remove
236 carbonates prior to element and isotopic analyses at the State Key Laboratory of Isotope
237 Geochemistry, Guangzhou Institute of Geochemistry, Chinese Academy of Sciences.
238 Trace elements of all the samples were measured on a Perkin-Elmer Sciex Elan 6000
239 inductively coupled plasma mass spectrometer (ICP-MS). Sr and Nd isotopic ratios of
240 sixty samples were analyzed on a MicroMass Isoprobe multicollector inductively coupled
241 plasma mass spectrometer (MC-ICP-MS). The $^{87}Sr/^{86}Sr$ ratios of thirteen samples could
242 not be measured because we failed to separate Sr from these samples. Analytical methods
243 are provided in full in Supplementary Materials.

244

245 ## 4. Results

246 Results of the trace element and Sr-Nd isotopic analyses of the silicate fraction of
247 the Nicobar Fan samples are listed in Supplementary Tables A.1 and A.2, respectively.

4.1.Trace elements

The trace elements Rb, Th, Ta, Nb, Y, show higher concentrations in our samples compared to the Upper Continental Crust (UCC) (Rudnick and Gao, 2003) (Fig. 3a). Abundances of transitional elements, V, Sc, Co, Cr and Ni in the Nicobar Fan samples are also higher than those of the UCC (Fig. 3a). Most samples share similar pattern of trace elements, except that Co and Ni abundances show a considerably scatter and are significantly higher in Unit IIIA than in Units I and II. In general, trace elements in the Nicobar Fan samples show similar characteristics to those in the Himalayan-derived Neogene Surma Basin and Bengal Fan sediments (Hossain et al., 2010; Crowley et al., 1998), although Ta, Zr and Hf concentrations in the Surma Basin sediments are obviously higher than those in the Nicobar Fan samples (Fig. 3a). Chondrite-normalized distribution patterns of rare earth element (REE) concentrations in the Nicobar Fan samples are similar to those of the UCC, as well as Neogene Surma Basin and Bengal Fan sediments, in displaying light REEs enrichment, heavy REEs depletion and a negative Eu anomaly (Fig. 3b). Temporal variations of element contents and ratios however show an abrupt change at ~9.2 Ma (boundary of Units II and IIIA) at both Sites U1480 and U1481, characterized by marked rise in Th, Ta and Nb contents and La/Lu and La_N/Yb_N ratios but significant drop in Cr/Th ratio (Fig. 4). Although highly variable in terms of these element contents and ratios since ~9.2 Ma, the Unit II sediments overall show higher Th, Ta and Nb contents, higher La/Lu and La_N/Yb_N ratios but lower Cr/Th ratio than those of the Unit IIIA sediments.

4.2.Sr and Nd isotopes

The $^{87}Sr/^{86}Sr$ ratios of the Nicobar Fan samples vary from 0.719718 to 0.750453 (Table A.2). The Unit IIIA sediments show relatively uniform $^{87}Sr/^{86}Sr$ ratios ranging from 0.721300 to 0.731113 (average of 0.726131), which then increased rapidly and concurrently by 0.03 units after ~9.2 Ma (the Units II and IIIA boundary) at both Sites U1480 and U1481 (Fig. 5). Although highly variable between 0.723152 and 0.750453, the $^{87}Sr/^{86}Sr$ ratios of the Unit II sediments (average of 0.734478) are generally higher than those of the Unit IIIA sediments. However, the Unit I sediments have an average $^{87}Sr/^{86}Sr$ ratios of 0.722044, close to the Unit IIIA average.

The ε_{Nd} values range from -16.1 to -7.8 (Table A.2), and the temporal evolution is negatively correlated with the $^{87}Sr/^{86}Sr$ ratios (Fig. 5). The Unit IIIA sediments have higher ε_{Nd} values, ranging from -13.3 to -7.8 (average of -11.7), whereas the Unit II sediments generally have lower ε_{Nd} values (average of -13.5) highly oscillating between -16.1 and -10.5. An oscillatory decrease in ε_{Nd} values is observed around the Units II and IIIA boundary (Fig. 5). The ε_{Nd} values decreased from -12.2 at 9.24 Ma to -14.7 at 8.76 Ma at Site U1480, while it first increased from -11.9 at 9.26 Ma to -10.1 at 9.18 Ma but then dropped to -14.8 at 8.72 Ma at Site U1481. The ε_{Nd} values of the Unit I samples are concentrated in the range of -11.5 to -10.6 (average of -11.1).

The Nicobar Fan sediments overall exhibit negative correlations between ε_{Nd} versus Th, Ta and Nb contents and La/Lu and La_N/Yb_N ratios, and a positive correlation between ε_{Nd} versus Cr/Th ratio (Fig. 6). Because Nd isotopes are not modified by mineral sorting processes, we deduce that these trace element contents and ratios are not significantly

affected by mineral sorting but primarily controlled by the composition of the source areas (the Himalaya and the Gangdese arc as discussed below).

5. Discussion

5.1.Eastern Himalayan Provenance for the Nicobar Fan sediments

The trace element and REE distribution patterns of the Nicobar Fan sediments denote a Himalayan provenance dominated by sedimentary-metasedimentary rocks. However, enrichment of the transitional elements relative to UCC indicates additional input of more mafic rocks. The Niocbar Fan sediments also reflect mixing between felsic and intermediate sources on a plot of Cr/Th versus Th/Sc (Fig. A.1). It is also noteworthy that the Nicobar Fan sediments show higher ε_{Nd} values and lower $^{87}Sr/^{86}Sr$ ratios than contemporary sediments in the Bengal Fan (France-Lanord et al., 1993; Galy et al., 1996; Galy et al., 2010), the Nepalese foreland (Huyghe et al., 2001, 2005; Szulc et al., 2006), and the eastern Himalayan foreland (Chirouze et al., 2013) through the Neogene (Fig. 5). The fan sediments also have higher ε_{Nd} values and lower $^{87}Sr/^{86}Sr$ ratios than the Surma Basin sediments in the Miocene (Bracciali et al., 2015) (Fig. 5). Here we employ a Sr-Nd isotope diagram to distinguish the possible sources for the Nicobar Fan (Fig. 7a). To understand the source-to-sink process from the Himalaya to the northeastern Indian Ocean, we also compare Sr-Nd isotope compositions of the Nicobar Fan sediments with those of modern sediments in the Ganges and Brahmaputra mainstreams upstream their confluence in the Bengal delta (Singh and France-Lanord, 2002; Singh et al., 2008).

The Brahmaputra sediments have obviously higher ε_{Nd} values and lower $^{87}Sr/^{86}Sr$ ratios than the Ganges sediments (Table 1). They are separate from each other in the Sr-Nd isotope diagram (Fig 7a). Such distinction reflects contributions from their drainage basins. The Ganges River drains the central Tethyan, Greater and Lesser Himalayas as well as peninsular India. Of these, the Greater and Lesser Himalayas make up most of the sediment load of the Ganges River, with the Greater Himalaya contributing >65% of the total (Singh et al., 2008). Sediment input from the Tethyan Himalaya lying in the rain shadow and from peninsular India is estimated to be minor (Singh et al., 2008). The Brahmaputra River drains the same units in the eastern Himalaya, with its upper reach, the Yarlung Tsangpo, draining the Tethyan Himalaya and the Gangdese arc. Therefore, the Brahmaputra River is characterized by significant input from the Gangdese arc, whereas the Ganges River shows more input from the Lesser Himalaya (Fig 7a). The Sr-Nd isotope compositions of the Nicobar Fan sediments are close to the field of the Brahmaputra sediments with slightly higher ε_{Nd} values (Fig 7a), showing Greater Himalayan affinity plus a significant Gangdese arc contribution, which could account for enrichment of the transitional elements.

Although the Burmese arc has similar Sr-Nd isotope compositions to the Gangdese arc (Table 1 and Fig 7a), it could not be the major contributor to the arc components in the Nicobar Fan. Direct input from the Burmese arc to the Nicobar Fan is unlikely, because the accretionary prism (the Paleogene Indo-Burman Ranges) was uplifted and emerged around 39–37 Ma, as evidenced by the quasi-closed estuarine condition and the shift from westward-directed deltaic system to southward-directed fluvial-deltaic system in the forearc basin (the western Central Myanmar Basin) at that time (Licht et al., 2016;

2018). The Paleogene Indo-Burman Ranges would thus have provided a barrier to transport of the Burmese arc material westward. Therefore, during the Neogene, the Burmese arc material would have been delivered by the Irrawaddy River flowing southward along the Central Myanmar Basin and finally been trapped in the Martaban Basin (Racey and Ridd, 2015). Although sediments from the arc-derived Paleogene Indo-Burman Ranges were regarded as a significant contributor to the eastern Bay of Bengal in the last glacial-interglacial cycle when the eastern Bengal Fan was inactive, they were speculated to be transported by ocean surface currents driven by monsoon winds (e.g. Colin et al., 1999; Joussain et al., 2016). The Nicobar Fan was active during 19–1.7 Ma and dominated by sandy and muddy turbidites (Pickering et al., 2020), which were primarily advected by turbidite currents instead of surface currents. It is obvious that the small rivers draining the western flank of the Indo-Burman Ranges could not supply turbidites to the distant Nicobar Fan sites. Moreover, the anticyclonic/cyclonic surface circulation driven by summer/winter monsoons in the Bay of Bengal are restricted north of 12°N (e.g. Joussain et al., 2016). We thus do not expect that the Paleogene Indo-Burman Ranges material would reach the Nicobar Fan sites near the Equator today and in the Southern Hemisphere during the Miocene (Hall, 2012) (Fig. 8). Therefore, we exclude that the arc components in the Nicobar Fan were recycled from the Paleogene Indo-Burman Ranges.

The Nicobar Fan sediments also overlap the range of Neogene sediments in the Surma Basin which represent the paleo-Brahmaputra deposits (Bracciali et al., 2015). The close affinity in Sr-Nd isotope compositions between the Nicobar Fan, the Surma Basin and the Brahmaputra sediments implies that the Nicobar Fan sediments were primarily

360 supplied by the Brahmaputra River from the eastern Himalaya. Unlike the Nicobar Fan
361 sediments, Sr-Nd isotope compositions of the Bengal Fan sediments overlap both the
362 ranges of the Brahmaputra and the Ganges sediments (Fig. 7a), indicating a mixture of
363 sediments derived from the two rivers. The Nepalese foreland sediments have most
364 affinity with the Ganges sediments, displaying significant Lesser Himalaya input, as
365 expected (Fig. 7a). Mixing of the Ganges and Brahmaputra sediments in various
366 proportions in the Bengal Fan during the Neogene has also been demonstrated by detrital
367 zircon U-Pb dating from Bengal Fan IODP sites (Blum et al., 2018). In light of the
368 temporal variation in detrital U-Pb age populations, the Ganges River is known to have
369 served as the major source of sediment to the Bengal Fan prior to ~3.5 Ma, although it is
370 nowadays mostly supplied by the Brahmaputra River (Blum et al., 2018). The difference
371 in Sr-Nd isotope compositions between the Bengal Fan and the Nicobar Fan sediments
372 implies that the Ganges and the Brahmaputra Rivers used to deliver sediments separately
373 to the Bay of Bengal through independent river mouths and slope canyon-channel
374 systems (Fig. 8). Mixing of Ganges and Brahmaputra sediments by channel avulsions
375 appears to have been common in the Bengal Fan, but not in the Nicobar Fan, or the
376 Nicobar Fan sediments would also plot between the Ganges and the Brahmaputra
377 sediments in the Sr-Nd isotope diagram. Separation of the Ganges-Brahmaputra river
378 mouths is evidenced by a paleo-Brahmaputra course east of the Shillong Plateau, which
379 was redirected west by the rising plateau and the westward-propagated Indo-Burman
380 Ranges at 5.2–4.9 Ma (Govin et al., 2018) (Figs. 8b and 8c). However, it remains
381 unknown when the two rivers first joined after then as river avulsion might occurred
382 frequently. Some clues indicate that the Ganges-Brahmaputra River mouths were still

383 separated at times during the Quaternary. For example, distribution of the Bengal Fan
384 sequences suggests two active canyon-channel systems during 1.9–0.96 Ma (Curray et al.,
385 2003), which were probably fed by the Ganges River and Brahmaputra River respectively.
386 Therefore, compared to the Bengal Fan, the Nicobar Fan provides a simpler erosion
387 record of the eastern Himalaya that can be used to constrain the timing of integration of
388 the Yarlung Tsangpo-Brahmaputra River and initiation of the rapid syntaxial exhumation.

389

390 *5.2.An integrated Yarlung Tsangpo-Brahmaputra River since Early Miocene*

391 The Sr-Nd isotope compositions of the Nicobar Fan sediments indicate an eastern
392 Himalayan source dominated by the Greater Himalaya but with significant Gangdese arc
393 contribution since ~19 Ma. It is noteworthy that the arc component in Unit IIIA is
394 stronger than that in Unit II, as indicated by the significantly higher Co and Ni contents
395 (Fig. 3a), lower Th, Ta and Nb contents, lower La/Lu and La_N/Yb_N ratios and higher
396 Cr/Th ratios (Fig. 4), as well as higher ε_{Nd} values and lower $^{87}Sr/^{86}Sr$ ratios (Figs. 5 and
397 7). The Unit IIIA sediments also show higher ε_{Nd} values (-13.3 to -7.8) than modern
398 Brahmaputra sediments (-16.9 to -12.5) (Fig. 7a). Because Gangdese arc material in the
399 Brahmaputra River is presently strongly diluted by the Greater Himalayan detritus
400 derived from the rapidly exhuming eastern Himalayan syntaxis, the higher ε_{Nd} values
401 seen in Unit IIIA sediments at 19–9.2 Ma could reflect the Brahmaputra sedimentation
402 prior to rapid syntaxial exhumation. Determining the proportions of the Greater Himalaya
403 and the Gangdese arc contributing to the Nicobar Fan might be complex, because the
404 Lesser and Tethyan Himalayas would be part of the source mixture although their
405 contributions are minor. Nevertheless, we perform a simple two-components mixing

406 model based on Sr-Nd isotopes only regarding the Greater Himalaya and the Gangdese
407 arc (Fig. 7b). In this model, the proportion of the Gangdese arc material could be over
408 ~50% in average in the Unit IIIA sediments (Fig. 7b).

409 Airfall volcanic ash is occasionally found through Unit IIIA in form of very thin
410 (0.5–4 cm) ash layers (McNeill et al., 2017a), but we avoided collecting samples from
411 these layers. Except for a single sample (~16.7 Ma) with a high ε_{Nd} value (-7.8) (Fig. 5),
412 the Unit IIIA sediments show relatively stable $^{87}Sr/^{86}Sr$ ratios, ε_{Nd} values and element
413 concentrations and ratios at both Sites U1480 and U1481, indicating a long-term
414 continuous input from the Gangdese arc and no significant dispersed volcanic ash in the
415 samples. Moreover, the sample with a high ε_{Nd} value (-7.8) was collected from silty
416 mudstone within turbidite units, which obviously lack of volcanic ash. All the evidence
417 above suggests that igneous detritus instead of volcanic ash is responsible for the
418 geochemical characteristic of the Unit IIIA sediments.

419 The influence of Gangdese arc detritus in the Nicobar Fan is also supported by the
420 presence of typical Cretaceous–Eocene Gangdese zircons (Govin et al., 2018) throughout
421 the core samples, with the proportion of <150 Ma population ranging 2–17% (McNeil et
422 al., 2017b) (Fig. 5). The oldest sediments (~18 Ma) in Site U1451 on the Bengal Fan also
423 show 8% zircon grains of <150 Ma population (Blum et al., 2018). As the 75–50 Ma
424 population is absent in the Himalayan units and rare in the Bomi-Chayu batholith east of
425 the syntaxis, it can be regarded as an exclusive indicator of the Gangdese arc (Bracciali et
426 al., 2015; Lang and Huntington, 2014). This age population is found in the Nicobar Fan
427 sediments, particularly in the Lower Miocene sample, although only at <6% of the total
428 population (Fig. 5). Therefore, the detrital geochronology, along with our Sr-Nd isotope

results, show long-term continuous input from the Gangdese arc to the Nicobar Fan via the Brahmaputra River. We thus propose an integrated Yarlung Tsangpo-Brahmaputra River being active at least since the Early Miocene (~19 Ma) (Fig. 8a). This timing is compatible with the results from the eastern Himalayan foreland near the Siang River (Lang and Huntington, 2014) and from the Surma Basin (Bracciali et al., 2015), suggesting connection of the Yarlung Tsangpo-Brahmaputra River through the Siang River. Importantly, we provide improved age constraints because the depositional age of the fluvial deposits is difficult to accurately determine. Our result also demonstrates the diachronous arrival of Gangdese arc detritus in the eastern Himalayan foreland, which was dated as ~10 Ma in the Subansiri River section (Cina et al., 2009), ~7 Ma in the Kameng River section (Chirouze et al. 2013) and ~5 Ma farther west (Govin et al., 2018), arose from the westward migration of the Brahmaputra course (Govin et al., 2018). However, whether and when the Yarlung Tsangpo was captured by the Brahmaputra River remains ambiguous. Bracciali et al. (2015) found no detrital zircons of Gangdese-age in two Upper Eocene–Oligocene samples in the Surma Basin. Based on the sedimentary records in the Central Myanmar Basin, Robinson et al. (2014) proposed that a Yarlung Tsangpo-Irrawaddy River was established by 40 Ma and was then captured by the Brahmaputra River before the Early Miocene. In contrast, Licht et al. (2016) found no evidence to support a Yarlung Tsangpo-Irrawaddy connection. This might infer a long-lived Yarlung Tsangpo-Brahmaputra River that was established before the Early Miocene, and it is possible that the Brahmaputra River drained east of the Surma Basin at that time.

5.3.Two-stage rapid exhumation of the eastern Himalayan syntaxis since Late Miocene

The noteworthy increase in sedimentation rate at the Nicobar Fan sites at ~9.2 Ma was interpreted as the result of the reduction in accommodation space of the Bengal Basin due to the inversion of the Shillong Plateau and the westward encroachment of the Indo-Burma Ranges, which increased sediment supply directly to the Nicobar Fan (McNeil et al., 2017b). However, although the exhumation of the Shillong Plateau begun at 15–9 Ma (Biswas et al., 2007), topographic growth of the plateau was chronologically decoupled from the exhumation and did not initiate until 5.2–4.9 Ma (Govin et al., 2018) owing to the contrasting erodibility between the sedimentary cover and the resistant basement rocks (Biswas et al., 2007). The growth history of the Indo-Burma Ranges has not yet been accurately dated. Thus, the sedimentation rate variation at ~9.2 Ma is hard to be interpreted as a reflection of the reduction in continental accommodation space. Synchronous with the acceleration in sedimentation rate, the abrupt change in trace element contents and ratios and Sr-Nd isotope compositions around 9.2 Ma denotes a provenance shift (Figs. 4 and 5). The decreasing ε_{Nd} values and increasing $^{87}Sr/^{86}Sr$ ratios implies increasing flux of Greater and/or Lesser Himalayan material compared to Gangdese arc sediments (Fig. 7a). Although the increase of Lesser Himalayan detritus in response to the Lesser Himalayan exhumation was proposed in the western and central Himalayan forelands at 12–10 Ma (Huyghe et al., 2001; Szulc et al., 2006), it has not yet been documented in the eastern Himalayan foreland. The Lesser Himalaya could not be the primary source leading to the sediment geochemistry and sedimentation rate changes of the Nicobar Fan at ~9.2 Ma. If that was the case then post-9.2 Ma sediments would show extremely low ε_{Nd} values and high $^{87}Sr/^{86}Sr$ ratios like the Nepalese foreland under such accelerating sedimentation rate (Fig. 7a).

475 Instead, we ascribe the changes in sediment geochemistry and sedimentation rate at
476 ~9.2 Ma to an increase in the flux of Greater Himalayan material (the proportion
477 increased from ~50% in Unit IIIA to ~70% in Unit II, Fig. 7b) linked to the rapid
478 exhumation of the Greater Himalayan crystalline rocks in the eastern Himalayan syntaxis
479 (Fig. 8b). This conclusion is also supported by the detrital apatite fission-track data from
480 the Nicobar Fan; apatite grains with short (<1 m.y. and even zero) lag times indicating
481 rapid source-area exhumation were observed at 9–2 Ma (Pickering et al., 2018). Initiation
482 of rapid syntaxial exhumation as reflected in the Nicobar Fan sediments (~9.2 Ma) is
483 consistent with the older onset ages, ~11–9.7 Ma (Ding et al., 2001; Booth et al., 2004)
484 and ~10 Ma (Zeitler et al., 2014), determined from the bedrock thermochronology and
485 geochronology. It is also compatible with the poorly dated constraints from detrital
486 thermochronology from the foreland sections downstream the Siang River, of 7–5 Ma or
487 earlier (Lang et al., 2016). Zeitler et al. (2014) proposed that rapid exhumation starting
488 from ~10 Ma took place in a broad syntaxial region including the easternmost Lhasa
489 block (Fig. 8b). The variations of the Sr-Nd isotope compositions and the sedimentation
490 rate in Unit II suggest that the rapid syntaxial exhumation was likely to have reduced
491 around 6–5 Ma (Fig. 5), in agreement with the model proposed by Zeitler et al. (2014).

492 An interval of very low ε_{Nd} values (-14 to -16) and high $^{87}Sr/^{86}Sr$ ratios (0.74 to 0.75)
493 in the Nicobar Fan sediment is observed again at 3.5–1.7 Ma when sedimentation rates
494 reached a peak of ~290 m/m.y. (Fig. 5) before Pleistocene fan abandonment. The
495 proportion of the Greater Himalayan material increase up to ~80% (Unit IIA average in
496 Fig. 7b). This episode is coeval with the previously proposed younger onset age of the
497 syntaxial exhumation at ~3.5 Ma based on most of the bedrock thermochronology data

(e.g. Burg et al., 1997; Seward and Burg, 2008). This younger pulse of rapid exhumation since ~3.5 Ma was stronger but only focused in the Namche Barwa massif, defined as the core of the syntaxis northeast of the Nam La Thrust (Zeitler et al., 2014) (Fig. 8c). It is also witnessed in the Bengal Fan and the Surma Basin, as evidenced by the presence of detrital minerals with <1 m.y. lag times since ~3.5 Ma (Najman et al., 2019; Bracciali et al. 2016). The absence of this signal of rapid syntaxial exhumation in the Bengal Fan between 9.2 and 3.5 Ma might be due to strong supply of the Ganges sediments to that depocenter (Blum et al., 2018). The variations in sediment geochemistry and sedimentation rate seen at ~9.2 Ma in the Nicobar Fan were not observed in the Bengal Fan sites either. The stronger exhumation pulse since ~3.5 Ma enabled more Brahmaputra sediments to be delivered into the Bengal Fan (Fig. 8c), as indicated by the increase of Gangdese-age zircons and the first appearance of short-lag time minerals (Blum et al., 2018; Najman et al., 2019). However, it is puzzling that the signal of rapid syntaxial exhumation did not appear until 3.5–2.0 Ma in the Surma Basin, at odds with the presence of Gangdese arc material since the Early Miocene (Bracciali et al., 2015, 2016). This mis-match might result from the effects of dilution, hydraulic sorting and grain size.

The sedimentary record from the Nicobar Fan favors a two-stage exhumation model of the eastern Himalayan syntaxis. Despite the sedimentation rate and provenance variations, more specific detrital thermochronological work needs to be done on the Nicobar Fan to test this model. Regardless of whether the rapid syntaxial exhumation initiated at ~9.2 Ma or ~3.5 Ma these times significantly postdated the integration of the Yarlung Tsangpo-Brahmaputra River before ~19 Ma. If the capture of the Yarlung

521 Tsangpo by the Brahmaputra River occurred it would be at least 10 m.y. older than the
522 inception of rapid exhumation. Therefore, drainage capture followed by focused incision
523 cannot be responsible for the initiation of the rapid syntaxial exhumation as proposed by
524 the tectonic aneurysm model (Zeitler et al., 2001). Instead, the rapid exhumation must
525 have been initiated by tectonic uplift driven by the northward indentation of the
526 northeastern corner of the Indian Plate (e.g. Burg et al., 1997; Seward and Burg, 2008;
527 Bendick and Ehlers, 2014), which also distorted the course of the antecedent Yarlung
528 Tsangpo-Brahmaputra River. The rock uplift, probably coupled with monsoon
529 precipitation, would have enhanced river incision. A positive feedback between tectonics
530 and erosion would thus have been established. Therefore, we do not exclude the tectonic
531 aneurysm model (Zeitler et al., 2001; 2004) as the primary mechanism for sustaining or
532 accelerating rapid syntaxial exhumation.

533

534 **6. Conclusions**

535 We conducted a provenance study on well-dated Nicobar Fan sediments (19 Ma–
536 Recent) using trace element and Sr-Nd isotopic methods. We provide new time
537 constraints for integration of the Yarlung Tsangpo-Brahmaputra River and initiation of
538 rapid exhumation of the eastern Himalayan syntaxis.

539 The trace element and REE distribution patterns of the Nicobar Fan sediments
540 indicate a Himalayan provenance. The Sr-Nd isotope compositions of the Nicobar Fan
541 sediments further show a close affinity with Brahmaputra sediments dominated by the
542 Greater Himalayan material but also with significant contributions from the Gangdese arc,

543 demonstrating that the Nicobar Fan sediments were primarily supplied by the
544 Brahmaputra River from the eastern Himalaya. The geochemical and Sr-Nd isotope
545 compositions of the lower part of the Nicobar Fan indicate long-term continuous input of
546 Gangdese arc material to the deep sea, and therefore imply an integrated Yarlung
547 Tsangpo-Brahmaputra River flowing at least since the Early Miocene (~19 Ma). Based
548 on variations in sedimentation rate and provenance of the Nicobar Fan, we favor a two-
549 stage rapid exhumation model of the eastern Himalayan syntaxis. The abrupt change in
550 geochemical and isotope compositions synchronous with the acceleration in
551 sedimentation rate at ~9.2 Ma indicates increasing flux of Greater Himalaya material in
552 response to the rapid exhumation commencing across a wide region of the eastern
553 Himalayan syntaxis. The very low ε_{Nd} values and high $^{87}Sr/^{86}Sr$ ratios at 3.5–1.7 Ma,
554 accompanying the peak sedimentation rate, corresponds to a younger pulse of rapid
555 exhumation focused in the core of the syntaxis since ~3.5 Ma. Because initiation of rapid
556 syntaxial exhumation postdated the integration of the Yarlung Tsangpo-Brahmaputra
557 River by at least 10 m.y., this must have been triggered by tectonic uplift instead of
558 capture of the Yarlung Tsangpo by the Brahmaputra River. A positive feedback between
559 tectonics and erosion would have been established subsequently.

560

561 **Acknowledgements**

562 This research used samples and data provided by the International Ocean Discovery
563 Program (IODP). We appreciate Science Party of IODP Expedition 362, in particular the
564 Co-Chief Scientists (McNeill L.C. and Dugan B.E.) and the Staff Scientist (Petronotis
565 K.E.), for their efforts. We also thank the IODP staff and JOIDES Resolution crew for

their contributions during the expedition. This research was financially supported by the National Natural Science Foundation of China (grant 41606068), research grants from the Key Special Project for Introduced Talents of Southern Marine Science and Engineering Guangdong Laboratory (Guangzhou) (GML2019ZD0202), the National Programme on Global Change and Air-Sea Interaction (GASI-GEOGE-02), and Innovation Academy of South China Sea Ecology and Environmental Engineering, Chinese Academy of Sciences (ISEE2020YB07), and the Research Fund Program of Guangdong Provincial Key Laboratory of Marine Resources and Coastal Engineering (grant GDKLMRCE1804). This is contribution IS-XXXX from GIGCAS. We thank Sun Shengling and Zhang Le for their help on the analyses in GIGCAS laboratories and thank Kutterolf Steffen for his helpful discussion. We are grateful to the editor and two anonymous reviewers for their valuable comments which have substantially improved the paper. All the data used in this paper are provided in Supplementary materials.

References

Allen, R., Najman, Y., Carter, A., Parrish, R., Bickle, M., Paul, M., Garzanti, E., Reisberg, L., Chapman, H., Vezzoli, G., Andò, S., 2008. Provenance of the Tertiary sedimentary rocks of the Indo-Burman Ranges, Burma (Myanmar): Burman arc or Himalayan-derived? J. Geol. Soc. London 165, 1045–1057. https://doi.org/10.1144/0016-76492007-143.

Backman, J., Chen, W., Kachovich, S., Mitchison, F., Petronotis, K., Yang, T., Zhao, X., 2019. Data report: revised age models for IODP Sites U1480 and U1481, Expedition 362， in: McNeill, L.C., Dugan, B., Petronotis, K.E., the Expedition 362

589 Scientists, Sumatra Subduction Zone. Proc. IODP, vol. 362. International Ocean
590 Discovery Program, College Station, TX.
591 https://doi.org/10.14379/iodp.proc.362.202.2019.
592 Bendick, R., Ehlers, T.A., 2014. Extreme localized exhumation at syntaxes initiated by
593 subduction geometry. Geophys. Res. Lett. 41(16), 5861–5867.
594 Biswas, S., Coutand, I., Grujic, D., Hager, C., Stöckli, D., Grasemann, B., 2007.
595 Exhumation and uplift of the Shillong plateau and its influence on the eastern
596 Himalayas: New constraints from apatite and zircon (U-Th-[Sm])/He and apatite
597 fission track analyses. Tectonics 26, TC6013.
598 Blum, M., Rogers, K., Gleason, J., Najman, Y., Cruz, J., Fox, L., 2018. Allogenic and
599 autogenic signals in the stratigraphic record of the deep-sea Bengal Fan. Sci. Rep. 8,
600 7973.
601 Booth, A.L., Zeitler, P.K., Kidd, W.S.F., Wooden, J., Liu, Y.P., Idleman, B., Hren, M.,
602 Chamberlain, C.P., 2004. U-Pb zircon constraints on the tectonic evolution of
603 southeastern Tibet, Namche Barwa area. Am. J. Sci. 304, 889–929.
604 Bracciali, L., Najman, Y., Parrish, R.R., Akhter, S.H., Millar, I., 2015. The Brahmaputra
605 tale of tectonics and erosion: Early Miocene river capture in the eastern Himalaya.
606 Earth Planet. Sci. Lett. 415, 25–37.
607 Bracciali, L., Parrish, R.R., Najman, Y., Smye, A., Carter, A., Wijbrans, J.R., 2016. Plio-
608 Pleistocene exhumation of the eastern Himalayan syntaxis and its domal ‘pop-up’.
609 Earth-Sci. Rev. 160, 350–385.
610 Brookfield, M.E., 1998. The evolution of the great river systems of southern Asia during
611 the Cenozoic India-Asia collision: Rivers draining southwards. Geomorphology 22,

612 285–312.
613 Burg, J.P., Davy, P., Nievergelt, P., Oberli, F., Seward, D., Diao, Z., Meier, M., 1997.
614 Exhumation during crustal folding in the Namche-Barwa syntaxis. Terra Nova 9,
615 53–56.
616 Chirouze, F., Huyghe, P., van der Beek, P., Chauvel, C., Chakraborty, T., Dupont-Nivet,
617 G., Bernet, M., 2013. Tectonics, exhumation, and drainage evolution of the eastern
618 Himalaya since 13 Ma from detrital geochemistry and thermochronology, Kameng
619 River Section, Arunachal Pradesh. Geol. Soc. Am. Bull. 125(3–4), 523–538.
620 Cina, S.E., Yin, A., Grove, M., Dubey, C.S., Shukla, D.P., Lovera, O.M., Kelty T.K.,
621 Gehrels G.E., Foster D.A., 2009. Gangdese arc detritus within the eastern
622 Himalayan Neogene foreland basin: Implications for the Neogene evolution of the
623 Yalu-Brahmaputra river system. Earth Planet. Sci. Lett. 285(1–2), 0–162.
624 Clark, M.K., Schoenbohm, L.M., Royden, L.H., Whipple, K.X., Burchfiel, B.C., Zhang,
625 X., Tang, W., Wang, E., Chen, L., 2004. Surface uplift, tectonics, and erosion of
626 eastern Tibet from large-scale drainage patterns. Tectonics 23(1), TC1006.
627 Colin, C., Turpin, L., Bertaux, J., Desprairies, A., Kissel, C., 1999. Erosional history of
628 the Himalayan and Burman ranges during the last two glacial–interglacial
629 cycles. Earth Planet. Sci. Lett. 171(4), 647–660.
630 Copeland, P., Harrison, T.M., Pan, Y., Kidd, W., Roden, M., Zhang, Y., 1995. Thermal
631 evolution of the Gangdese batholith, southern Tibet: a history of episodic un-roofing.
632 Tectonics 14, 223–236.
633 Crowley, S.F., Stow, D.A.V., Croudace, I.W., 1998. Mineralogy and geochemistry of Bay
634 of Bengal deep-sea fan sediments, ODP Leg 116: evidence for an Indian

635 subcontinent contribution to distal fan sedimentation, in: Cramp, A., MacLeod, C.J.,
636 Lee, S.V., Jones, E.J.W. (Eds.), Geological Evolution of Ocean Basins: Results from
637 the Ocean Drilling Program. Geol. Soc. London Spec. Publ. 131, 151–176.
638 Curray, J.R., Emmel, F.J., Moore, D.G., 2003. The Bengal Fan: morphology, geometry,
639 stratigraphy, history and processes. Mar. Petrol. Geol. 19(10), 1191–1223.
640 Ding, L., Zhong, D., Yin, A., Kapp, P., Harrison, T.M., 2001. Cenozoic structural and
641 metamorphic evolution of the eastern Himalayan syntaxis (Namche Barwa). Earth
642 Planet. Sci. Lett. 192, 423–438.
643 France-Lanord, C., Derry, L., Michard, A., 1993. Evolution of the Himalaya since
644 Miocene time: isotopic and sedimentological evidence from the Bengal Fan. Geol.
645 Soc. London Spec. Publ. 74(1), 603–621.
646 Frey, F.A., Silva, I.G.N., Huang, S., Pringle, M.S., Meleney, P.R., Weis, D. 2015.
647 Depleted components in the source of hotspot magmas: Evidence from the
648 Ninetyeast Ridge (Kerguelen). Earth and Planetary Science Letters, 426, 293-304.
649 Galy, A., France-Lanord, C., Derry, L.A., 1996. The Late Oligocene-Early Miocene
650 Himalayan belt constraints deduced from isotopic compositions of Early Miocene
651 turbidites in the Bengal Fan. Tectonophysics 260(1–3), 109–118.
652 Galy, V., France-Lanord, C., Peucker-Ehrenbrink, B., Huyghe, P., 2010. Sr-Nd-Os
653 evidence for a stable erosion regime in the Himalaya during the past 12 Myr. Earth
654 Planet. Sci. Lett. 290(3–4): 0–480.
655 Govin, G., Najman, Y., Copley, A., Millar, I., van der Beek, P., Huyghe, P., Grujic D.,
656 Davenport J., 2018. Timing and mechanism of the rise of the Shillong Plateau in the
657 Himalayan foreland. Geology 46 (3), 279–282.

658 doi: https://doi.org/10.1130/G39864.1
659 Hall, R., 2012. Late Jurassic–Cenozoic reconstructions of the Indonesian region and the
660 Indian Ocean. Tectonophysics 570–571, 1–41.
661 http://dx.doi.org/10.1016/j.tecto.2012.04.021.
662 Hossain, H.M.Z., Roser, B.P., Kimura, J.I., 2010. Petrography and whole-rock
663 geochemistry of the Tertiary Sylhet succession, northeastern Bengal Basin,
664 Bangladesh: Provenance and source area weathering. Sediment. Geol. 228(3–4),
665 171–183.
666 Huyghe, P., Galy, A., Mugnier, J. L., France-Lanord, C., 2001. Propagation of the thrust
667 system and erosion in the Lesser Himalaya: Geochemical and sedimentological
668 evidence. Geology 29(11), 1007–1010.
669 Huyghe, P., Mugnier, J.L., Gajurel, A.P., Delcaillau, B., 2005. Tectonic and climatic
670 control of the changes in the sedimentary record of the Karnali River section
671 (Siwaliks of western Nepal). Island Arc 14(4), 311–327.
672 Joussain, R., Colin, C., Liu, Z., Meynadier, L., Fournier, L., Fauquembergue, K.,
673 Zaragosi, S., Schmidt, F., Rojas, V., Bassinot, F., 2016. Climatic control of sediment
674 transport from the Himalayas to the proximal NE Bengal Fan during the last glacial-
675 interglacial cycle. Quaternary Sci. Rev. 148, 1–16.
676 Lang, K.A., Huntington, K.W., 2014. Antecedence of the Yarlung-Siang-Brahmaputra
677 River, eastern Himalaya. Earth Planet. Sci. Lett. 397, 145–158.
678 Lang, K.A., Huntington, K.W., Burmester, R., Housen, B, 2016. Rapid exhumation of the
679 eastern Himalayan syntaxis since the late Miocene. Geol. Soc. Am. Bull. 128(9),
680 1403–1422.

681 Licht, A., Reisberg, L., France-Lanord, C., Soe, A.N., Jaeger, J.J., 2016. Cenozoic
682 evolution of the Central Myanmar drainage system: insights from sediment
683 provenance in the Minbu Sub-Basin. Basin Res. 28(2), 237–251.
684 Licht, A., Dupont-Nivet, G., Win, Z., Swe, H.H., Kaythi, M., Roperch, P., Ugrai, T.,
685 Littell, V., Park, D., Westerweel, J., Jones, D., Poblete, F., Aung, D.W., Huang, H.,
686 Hoorn, C., Sein, K., 2018. Paleogene evolution of the Burmese forearc basin and
687 implications for the history of India-Asia convergence. Geol. Soc. Am. Bull. 131 (5-
688 6), 730–748. https://doi.org/10.1130/B35002.1.
689 Lin, T.H., Mitchell, A.H., Chung, S.L., Tan, X.B., Tang, J.T., Oo, T., Wu, F.Y., 2019. Two
690 parallel magmatic belts with contrasting isotopic characteristics from southern Tibet
691 to Myanmar: zircon U–Pb and Hf isotopic constraints. J. Geol. Soc. 176(3), 574–587.
692 McNeill, L.C., Dugan, B., Petronotis, K.E., the Expedition 362 Scientists, 2017a.
693 Sumatra Subduction Zone. Proc. IODP, vol. 362. International Ocean Discovery
694 Program, College Station, TX.
695 McNeill, L.C., Dugan, B., Backman, J., Pickering, K.T., Pouderoux, H.F.A., Henstock,
696 T.J., Petronotis, K.E., Carter, A., Chemale Jr., F., Milliken, K.L., Kutterolf, S.,
697 Mukoyoshi, H., Chen, W., Kachovich, S., Mitchison, F.L., Bourlange, S., Colson,
698 T.A., Frederik, M.C.G., Guèrin, G., Hamahashi, M., House, B.M., Hüpers, A.,
699 Jeppson, T.N., Kenigsberg, A.R., Kuranaga, M., Nair, N., Owari, S., Shan, Y., Song,
700 I., Torres, M.E., Vannucchi, P., Vrolijk, P.J., Yang, T., Zhao, X., and Thomas, E.,
701 2017b. Understanding Himalayan erosion and the significance of the Nicobar Fan.
702 Earth Planet. Sci. Lett. 475, 134–142.
703 Najman, Y., Mark, C., Barfod, D. N., Carter, A., Parrish, R., Chew, D., Gemignani, L.

2019. Spatial and temporal trends in exhumation of the Eastern Himalaya and syntaxis as determined from a multitechnique detrital thermochronological study of the Bengal Fan. Geol. Soc. Am. Bull. 131 (9–10), 1607–1622. https://doi.org/10.1130/B35031.1

Pickering, K.T., Pouderoux, H., Carter, A., Andò, S., Garzanti, E., Limonta, M., Vezzoli, G., Milliken, K.L., Chemale Jr., F., Mukoyoshi, H., Kutterolf, S. 2018. Sediment Provenance and Depositional History of the Nicobar Fan (Bengal Depositional System) from IODP Expedition 362: Detrital Zircon Geochronology, Apatite Thermochronometry, Sand Petrography and Heavy-Mineral Results. In AGU Fall Meeting Abstracts.

Pickering, K.T., Pouderoux, H., McNeill, L.C., Backman, J., Chemale, F., Kutterolf, S., Milliken, K.L., Mukoyoshi, H., Henstock, Timothy, J., Stevens, D.E., Parnell, C., Dugan, B., 2020. Sedimentology, stratigraphy and architecture of the Nicobar Fan (Bengal–Nicobar Fan System), Indian Ocean: Results from International Ocean Discovery Program Expedition 362. Sedimentology. doi: 10.1111/sed.12701.

Racey, A., Ridd, M.F., 2015. Petroleum geology of the Moattama region, Myanmar, in: Racey, A., Ridd, M.F. (Eds.), Petroleum geology of Myanmar. Geol. Soc. Lond. Mem. 45, pp. 63–81.

Robinson, R.A.J., Brezina, C.A., Parrish, R.R., Horstwood, M.S.A., Oo, N.W., Bird, M.I., Thein, M., Walters, A.S., Oliver, G.J.H., Zaw, K., 2014. Large rivers and orogens: The evolution of the Yarlung Tsangpo-Irrawaddy system and the eastern Himalayan syntaxis. Gondwana Res. 26(1), 112–121.

Rudnick, R.L., Gao, S., 2003. Composition of the continental crust, in: Rudnick, R.L.

(Ed.), Treatise on Geochemistry, vol. 3, The Crust. Elsevier, New York, pp. 1–64.

Seward, D., Burg, J. P., 2008. Growth of the Namche Barwa Syntaxis and associated evolution of the Tsangpo Gorge: constraints from structural and thermochronological data. Tectonophysics 451, 282–289.

Singh, S.K., France-Lanord, C., 2002. Tracing the distribution of erosion in the Brahmaputra watershed from isotopic compositions of stream sediments. Earth Planet. Sci. Lett. 202(3), 645–662.

Singh, S.K., Rai, S.K., Krishnaswami, S., 2008. Sr and Nd isotopes in river sediments from the Ganga Basin: Sediment provenance and spatial variability in physical erosion. J. Geophys. Res. Earth Surface, 113: F03006.

Sun, S.S., McDonough, W.S., 1989. Chemical and isotopic systematics of oceanic basalts: Implications for mantle composition and processes. Geol. Soc. London, Spec. Publ. 42(1), 313–345. https://doi.org/10.1144/GSL.SP.1989.042.01.19

Szulc, A.G., Najman, Y., Sinclair, H.D., Pringle, M., Bickle, M., Chapman, H., Garzanti E., Andò, DeCelles, P., 2006. Tectonic evolution of the Himalaya constrained by detrital ^{40}Ar-^{39}Ar, Sm-Nd and petrographic data from the Siwalik foreland basin succession, SW Nepal. Basin Res. 18(4), 375–391.

Wu, W., Xu, S., Yang, J., Yin, H., Lu, H., Zhang, K., 2010. Isotopic characteristics of river sediments on the Tibetan Plateau. Chem. Geol. 269(3–4), 406–413.

Yin, A., 2006. Cenozoic tectonic evolution of the Himalayan orogen as constrained by along-strike variation of structural geometry, exhumation history, and foreland sedimentation. Earth-Sci. Rev. 76(1–2), 1–131.

Zeitler, P.K., Meltzer, A.S., Koons, P.O., Craw, D., Hallet, B., Chamberlain, C.P., Kidd,

W.S.F., Park, S.K., Seeber, L., Bishop, M., Shroder, J., 2001. Erosion, Himalayan geodynamics, and the geomorphology of metamorphism. GSA Today 11: 4–8.

Zeitler, P.K., Meltzer, A.S., Brown, L., Kidd, W.S.F., Lim, C., Enkelmann, E., 2014. Tectonics and topographic evolution of Namche Barwa and the easternmost Lhasa Block, in: Nie, J., Hoke, G.D., Horton, B. (Eds.), Towards an Improved Understanding of Uplift Mechanisms and the Elevation History of the Tibetan Plateau. Spec. Pap., Geol. Soc. of Am. 507, 23–58.

Figure Captions (color online only for all figures)

Fig. 1. Regional map of the Bengal-Nicobar Fan system, showing the IODP Expedition 362 sites (U1480 and U1481) on the Nicobar Fan and the relevant drilling sites of DSDP Leg 22 (Site 218), ODP Leg 116 (Sites 717 and 718) and IODP Expedition 354 (Sites U1449–U1455). The superimposed simplified geological map of the eastern Himalaya, southeastern Tibet and Myanmar region, showing major terrains, terrain boundaries, geological units and modern major rivers, is modified from Robinson et al. (2014) and Licht et al. (2016). The Bengal Fan and the Nicobar Fan are outlined in black and grey, respectively (after Pickering et al., 2020). The Martaban basin in the eastern Andaman Sea is delineated by 3 km isopach (Racey and Ridd, 2015) in purple.

Fig. 2. Schematic lithological columns of Sites U1480 and U1481 modified from McNeill et al. (2017a), showing the position of the Nicobar Fan samples.

Fig. 3. (a) Upper continental crust (UCC) (Rudnick and Gao, 2003) normalized for trace

773 elements in the Nicobar Fan samples, as compared with the Neogene sediments of the
774 Surma Basin (Hossain et al., 2010) and the Bengal Fan (Crowley et al., 1998). (b)
775 Chondrite-normalized REE distribution plot for the Nicobar Fan samples as compared
776 with the UCC and the Neogene sediments of the Surma Basin (Hossain et al., 2010) and
777 the Bengal Fan (Crowley et al., 1998). The chondrite values are cited from Sun and
778 McDonough (1989).
779
780 **Fig. 4.** Downhole variation of Th, Ta and Nb concentrations, and Cr/Th, La/Lu and
781 La_N/Yb_N ratios of the Nicobar Fan sediments at both Sites U1480 and U1481. Age of the
782 Site U1480 and U1481 samples is converted from the mid-point depth according to age
783 models of Backman et al. (2019) and McNeil et al (2017a), respectively.
784
785 **Fig. 5.** Downhole variation of Sr-Nd isotopic compositions of the Nicobar Fan sediments
786 at both Sites U1480 and U1481, as compared with the Sr-Nd isotopic compositions of
787 contemporary sediments in the Bengal Fan (France-Lanord et al., 1993; Galy et al., 1996;
788 Galy et al., 2010), the Surma Basin (Bracciali et al., 2015), the eastern Himalayan
789 foreland (Chirouze et al., 2013) and the Nepalese foreland (Huyghe et al., 2001, 2005;
790 Szulc et al., 2006) and modern sediments in the Brahmaputra and the Ganges
791 mainstreams (Singh and France-Lanord, 2002; Singh et al., 2008). All the ε_{Nd} values and
792 $^{87}Sr/^{86}Sr$ ratios are recalculated at time T=0, and depositional ages of the Surma Basin
793 samples are of large uncertainties. Also shown are the sedimentation rate of Sites U1480
794 and U1481 (McNeill et al., 2017a, Backman et al., 2019), ODP Site 718C (after McNeill
795 et al., 2017b) and DSDP Site 218 (Galy et al., 2010), the proportion of detrital zircons

796 <150 Ma of the Nicobar Fan samples (McNeill et al. 2017b), and the associated
797 Himalayan tectonic events. GR=Ganges River, BR=Brahmaputra River, NER=Ninetyeast
798 Ridge.
799
800 **Fig. 6.** ε_{Nd} vs Th, Ta, Nb contents and Cr/Th, La/Lu and La_N/Yb_N ratios for the Niocbar
801 Fan samples. The grey dash lines in the plots represent the regression lines.
802
803 **Fig. 7.** (a) ε_{Nd} vs $^{87}Sr/^{86}Sr$ plot of the Nicobar Fan samples, as compared with the
804 potential source rocks from the Himalaya-Tibet region and the modern sediments in the
805 Brahmaputra and the Ganges mainstreams (see Table1 for references). The composition
806 fields of the Neogene sediments in the Bengal Fan, the Surma Basin and the Nepalese
807 foreland are also shown (France-Lanord et al., 1993; Galy et al., 1996; Galy et al., 2000;
808 Bracciali et al., 2015; Huyghe et al., 2001; 2005). (b) A simple two-components mixing
809 model based on Sr-Nd isotopes for the Nicobar Fan sediments. End-member
810 compositions used in the model are: the Greater Himalaya: Sr=70 ppm, Nd=45 ppm,
811 $^{87}Sr/^{86}Sr$=0.760, ε_{Nd}=-16 (Singh and France-Lanord, 2002; Singh et al., 2008); the
812 Gangdese arc: Sr=200 ppm, Nd=34 ppm; $^{87}Sr/^{86}Sr$=0.715; ε_{Nd}=-6.8 (Wu et al., 2010). The
813 latter is based on the average of the modem river sediments from the tributaries and
814 mainstream of the Yarlung Tsangpo that drain the southern Lhasa block. It should be
815 noted that in this calculation the proportion of the Gangdese arc also includes the Pre-
816 Cambrian basement rocks (the Nyainqêntanglha Group) and the Paleozoic–Mesozoic
817 sedimentary cover of the Lhasa block and even the Northern Magmatic belt intruded the
818 northern Lhasa block, besides the Cretaceous–Paleogene magmatic and volcanic rocks

819 (the Gangdese batholith and Linzizong volcanics) in the southern Lhasa block, because
820 the tributaries of the Yarlung Tsangpo also drain these units. This might be one of the
821 reasons why the proportion of Gangdese arc material derived from this model is much
822 higher than the proportion of typical Gangdese zircons (<150 Ma) in the Nicobar Fan
823 sand/sandstone (McNeil et al., 2017b) in Fig. 5 (other reasons might include the
824 abundance of zircons in parent rocks and hydraulic sorting of detrital zircons during
825 transport).
826
827 **Fig. 8.** Paleogeography reconstruction of the region of the northeastern Indian Ocean
828 (adapted from Hall, 2012), showing drainage evolution of the Ganges River and the
829 Yarlung Tsangpo-Brahmaputra River (modified from Lang and Huntington, 2014; Govin
830 et al., 2018) and the source-to-sink process from the Himalaya to the Bengal-Nicobar Fan
831 system. GR=Ganges River, BR=Brahmaputra River, IR=Irrawaddy River, SP=Shillong
832 Plateau, IBR=Indo-Burman Ranges, WPA=Wuntho-Popa Arc (Burmese arc),
833 NER=Ninetyeast Ridge.
834
835 **Tables**
836 Table 1. $^{87}Sr/^{86}Sr$ ratios and ε_{Nd} values of geologic units and major rivers of the Himalaya,
837 Tibet and Myanmar domain

Potential Source	$^{87}Sr/^{86}Sr$	ε_{Nd}	References
Himalaya and Tibet domain			
Lesser Himalaya	0.72–0.94	-25.3 to -23.5	Singh et al. (2008) and references therein
Greater Himalaya	0.73–0.79	-18 to -13.6	Singh and France-Lanord (2002); Singh et al. (2008) and references therein
Tethyan Himalaya	0.71–0.73	-15 to -12	Singh et al. (2008) and references therein
Gangdese arc (volcanics and granitoids in the southern Lhasa block)	0.70–0.73	-9 to +6	Wu et al. (2010) and references therein
Myanmar domain			

Paleogene Indo-Burman Ranges	0.714–0.716	-8.6 to -4.0	Colin et al. (1999); Allen et al. (2008)
Burmese arc (Wuntho-Popa Arc and intrusive rocks in Mogok Metamorphic Belt)	0.70–0.73	-10 to +4	Lin et al. (2019)
	Major Rivers		
Ganges River (mainstream)	0.748–0.787	-21.3 to -15.7	Singh et al. (2008)
Brahmaputra River (mainstream)	0.718–0.749	-16.9 to -12.5	Singh and France-Lanord (2002)
Irrawaddy River	0.713–0.714	-8.3 to -10.7	Colin et al. (1999); Allen et al. (2008)

838 *All the ε_{Nd} values and $^{87}Sr/^{86}Sr$ ratios are recalculated at time T=0.

839

840 **Appendix A. Supplementary materials**

841 Full Analytical Method

842 Table A.1. Trace elements of the Nicobar Fan sediments

843 Table A.2. Sr-Nd isotope composition of the Nicobar Fan sediments

844 Fig. A.1. Cr/Th versus Th/Sc diagram for the Nicobar Fan sediments

845

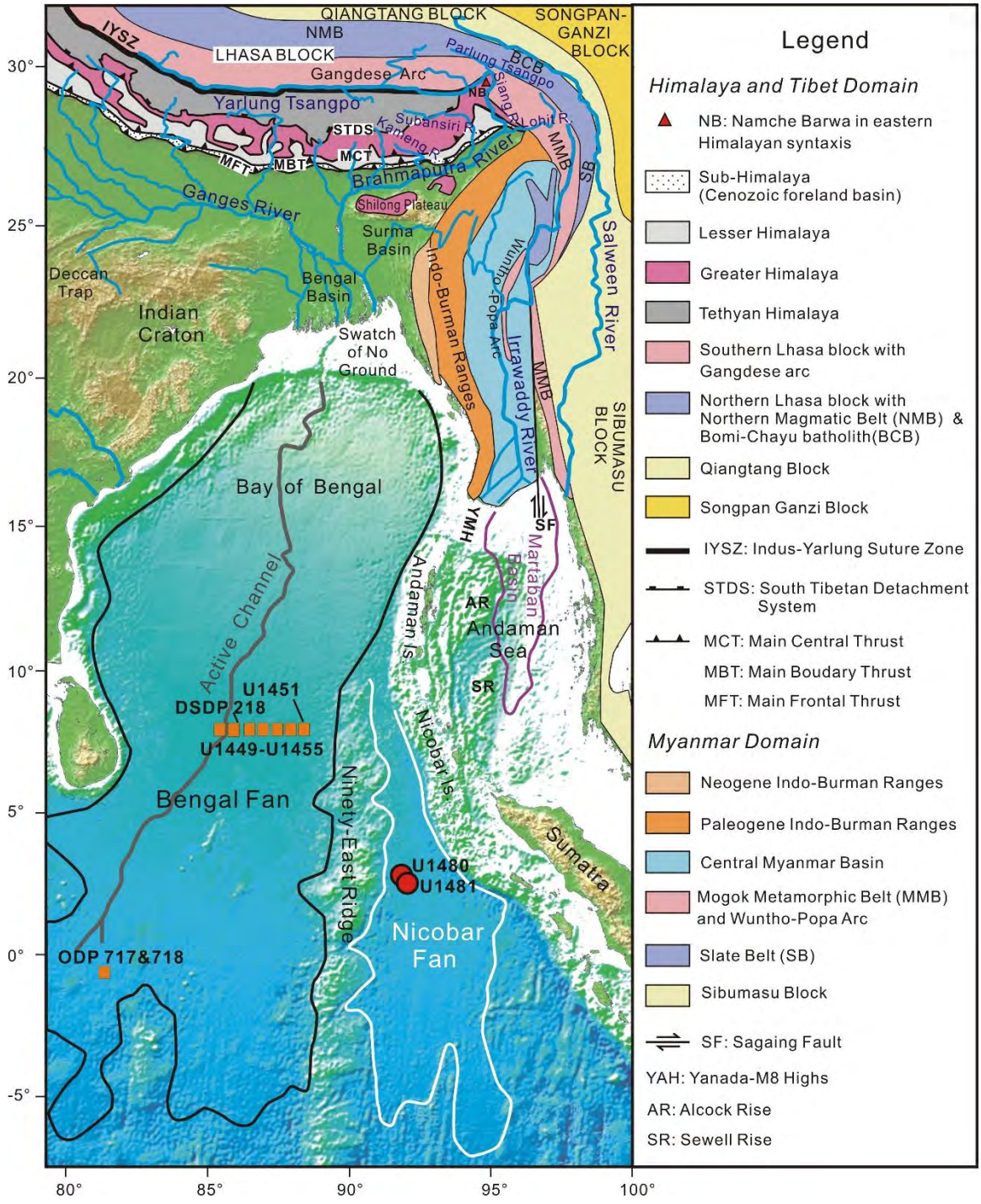
QIANGTANG BLOCK
SONGPAN-GANZI BLOCK
NMB
LHASA BLOCK
IYSZ
Gangdese Arc
Yarlung Tsangpo
Parlung Tsangpo
BCB
NB
Siang R.
Lohit R.
STDS
Subansiri R.
Kameng R.
MFT
MBT
MCT
MMB
SB
Brahmaputra River
Ganges River
Shilong Plateau
Surma Basin
Deccan Trap
Bengal Basin
Indian Craton
Swatch of No Ground
Indo-Burman Ranges
Wuntho-Popa Arc
Irrawaddy River
Salween River
SIBUMASU BLOCK
Bay of Bengal
YMH
SF
Martaban Basin
Andaman Is.
AR
Andaman Sea
Active Channel
SR
U1451
DSDP 218
U1449-U1455
Nicobar Is.
Bengal Fan
Ninety-East Ridge
Sumatra
U1480
U1481
Nicobar Fan
ODP 717&718
30°
25°
20°
15°
10°
5°
0°
-5°
80°
85°
90°
95°
100°
Legend
Himalaya and Tibet Domain
NB: Namche Barwa in eastern Himalayan syntaxis
Sub-Himalaya (Cenozoic foreland basin)
Lesser Himalaya
Greater Himalaya
Tethyan Himalaya
Southern Lhasa block with Gangdese arc
Northern Lhasa block with Northern Magmatic Belt (NMB) & Bomi-Chayu batholith(BCB)
Qiangtang Block
Songpan Ganzi Block
IYSZ: Indus-Yarlung Suture Zone
STDS: South Tibetan Detachment System
MCT: Main Central Thrust
MBT: Main Boudary Thrust
MFT: Main Frontal Thrust
Myanmar Domain
Neogene Indo-Burman Ranges
Paleogene Indo-Burman Ranges
Central Myanmar Basin
Mogok Metamorphic Belt (MMB) and Wuntho-Popa Arc
Slate Belt (SB)
Sibumasu Block
SF: Sagaing Fault
YAH: Yanada-M8 Highs
AR: Alcock Rise
SR: Sewell Rise

Fig. 1

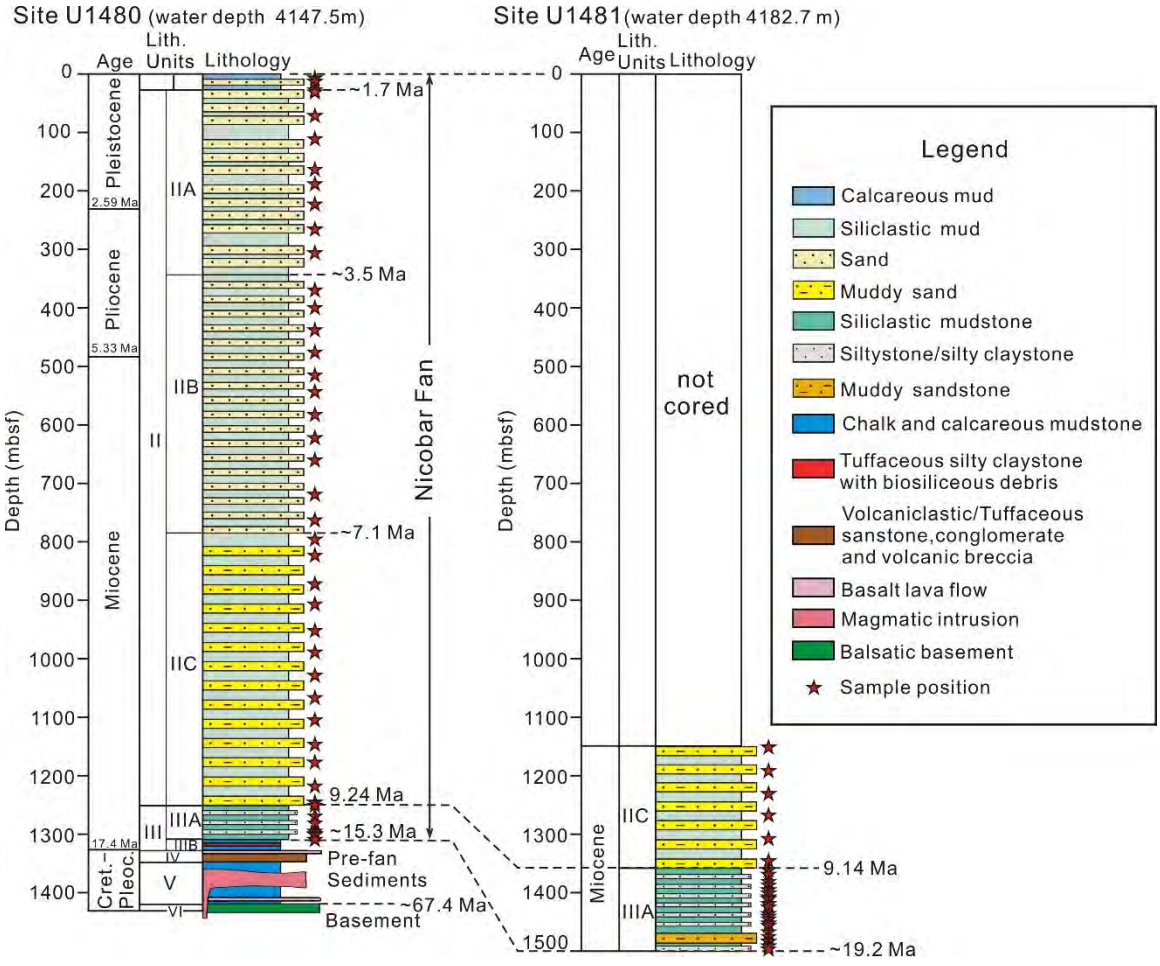

850

851 **Fig. 2**

852

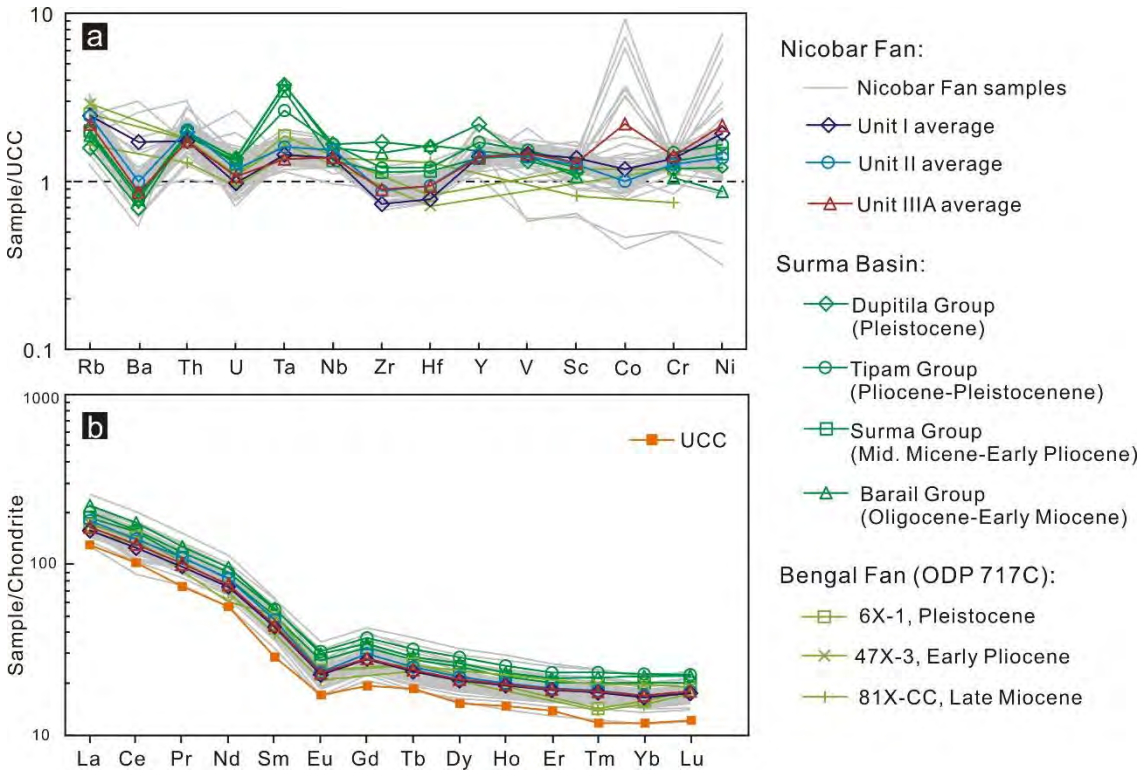

853

854 **Fig. 3**

855

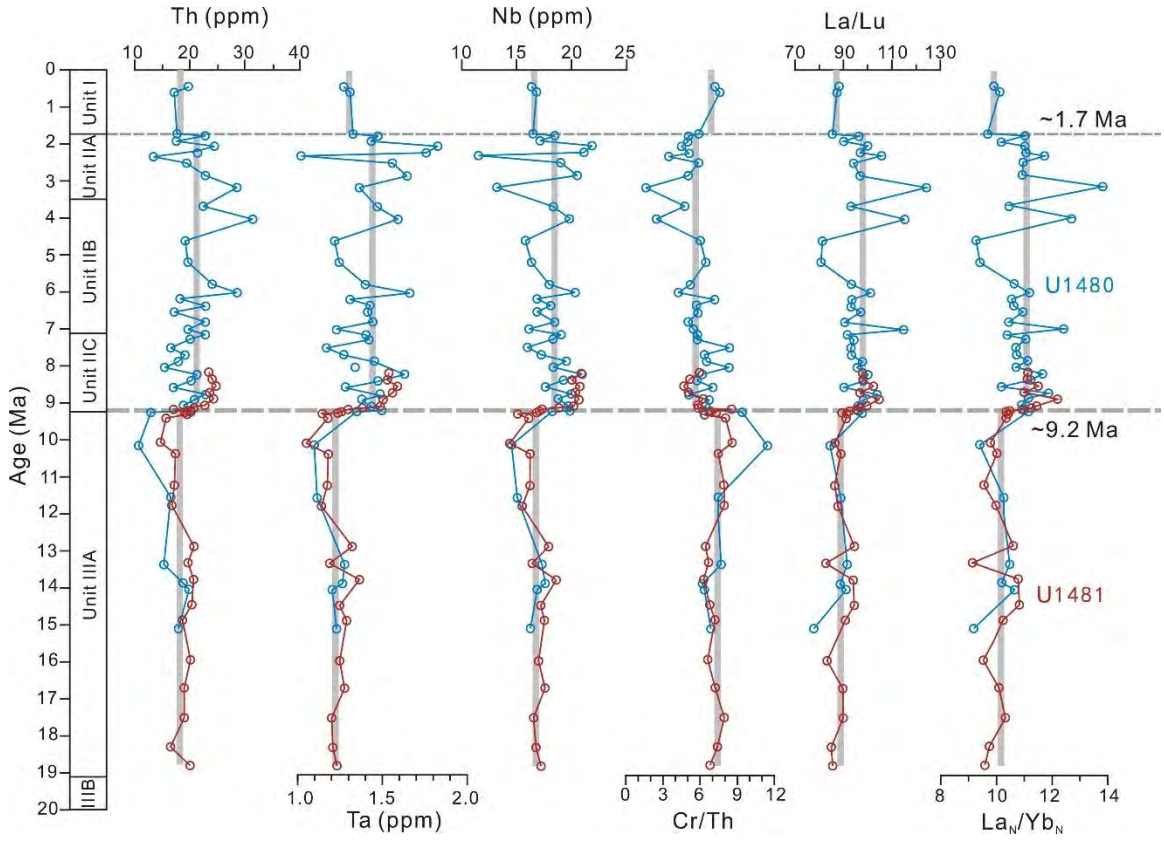

856

857 **Fig. 4**

858

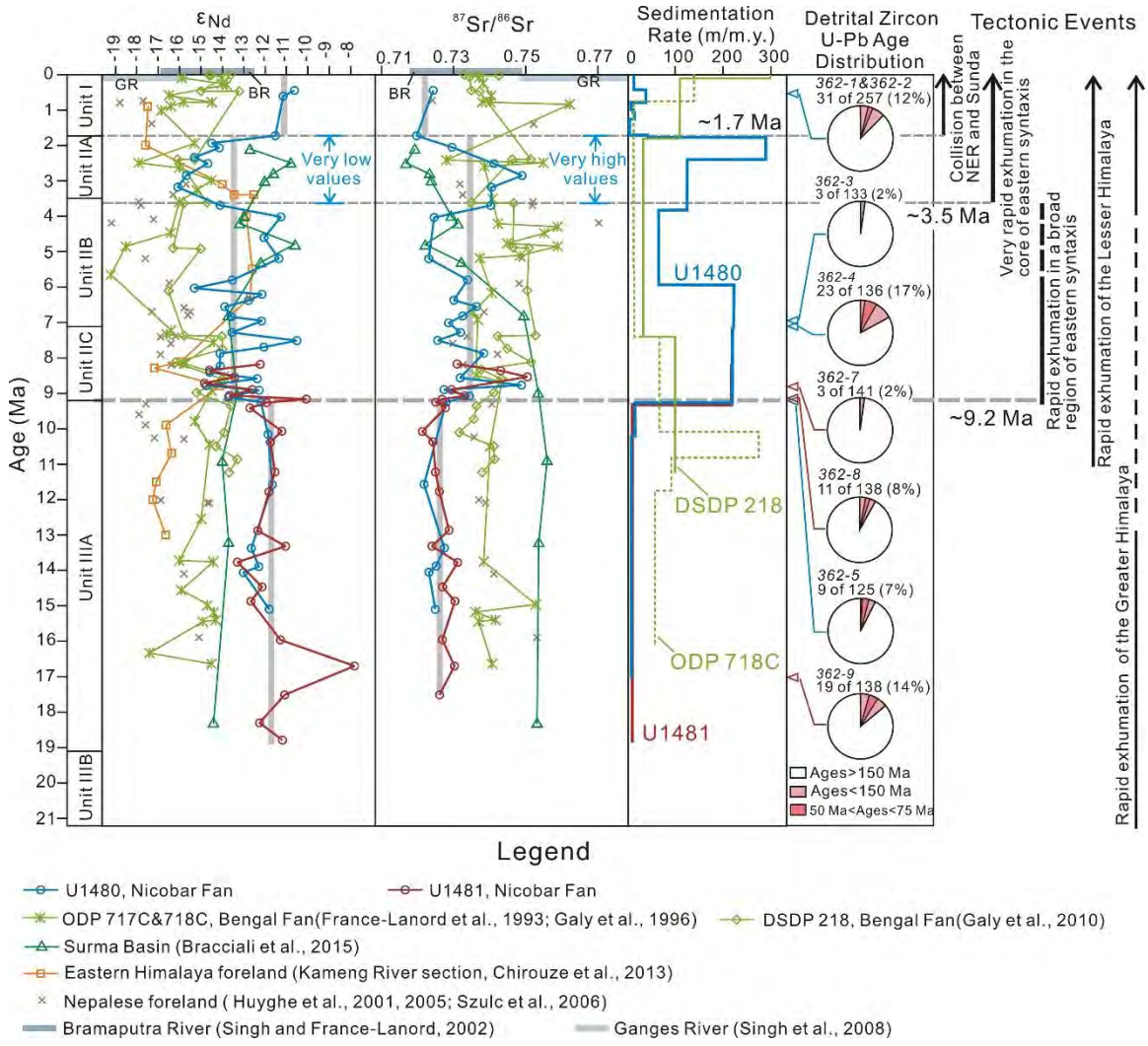
εNd
87Sr/86Sr
Sedimentation Rate (m/m.y.)
Detrital Zircon U-Pb Age Distribution
Tectonic Events
Age (Ma)
Unit I
Unit IIA
Unit IIB
Unit IIC
Unit IIIA
Unit IIIB
GR
BR
Very low values
Very high values
~1.7 Ma
U1480
DSDP 218
ODP 718C
U1481
362-1&362-2
31 of 257 (12%)
362-3
3 of 133 (2%)
362-4
23 of 136 (17%)
362-7
3 of 141 (2%)
362-8
11 of 138 (8%)
362-5
9 of 125 (7%)
362-9
19 of 138 (14%)
Ages>150 Ma
Ages<150 Ma
50 Ma<Ages<75 Ma
~3.5 Ma
~9.2 Ma
Collision between NER and Sunda
Very rapid exhumation in the core of eastern syntaxis
Rapid exhumation in a broad region of eastern syntaxis
Rapid exhumation of the Lesser Himalaya
Rapid exhumation of the Greater Himalaya
Legend
U1480, Nicobar Fan
U1481, Nicobar Fan
ODP 717C&718C, Bengal Fan(France-Lanord et al., 1993; Galy et al., 1996)
DSDP 218, Bengal Fan(Galy et al., 2010)
Surma Basin (Bracciali et al., 2015)
Eastern Himalaya foreland (Kameng River section, Chirouze et al., 2013)
Nepalese foreland (Huyghe et al., 2001, 2005; Szulc et al., 2006)
Bramaputra River (Singh and France-Lanord, 2002)
Ganges River (Singh et al., 2008)

Fig. 5

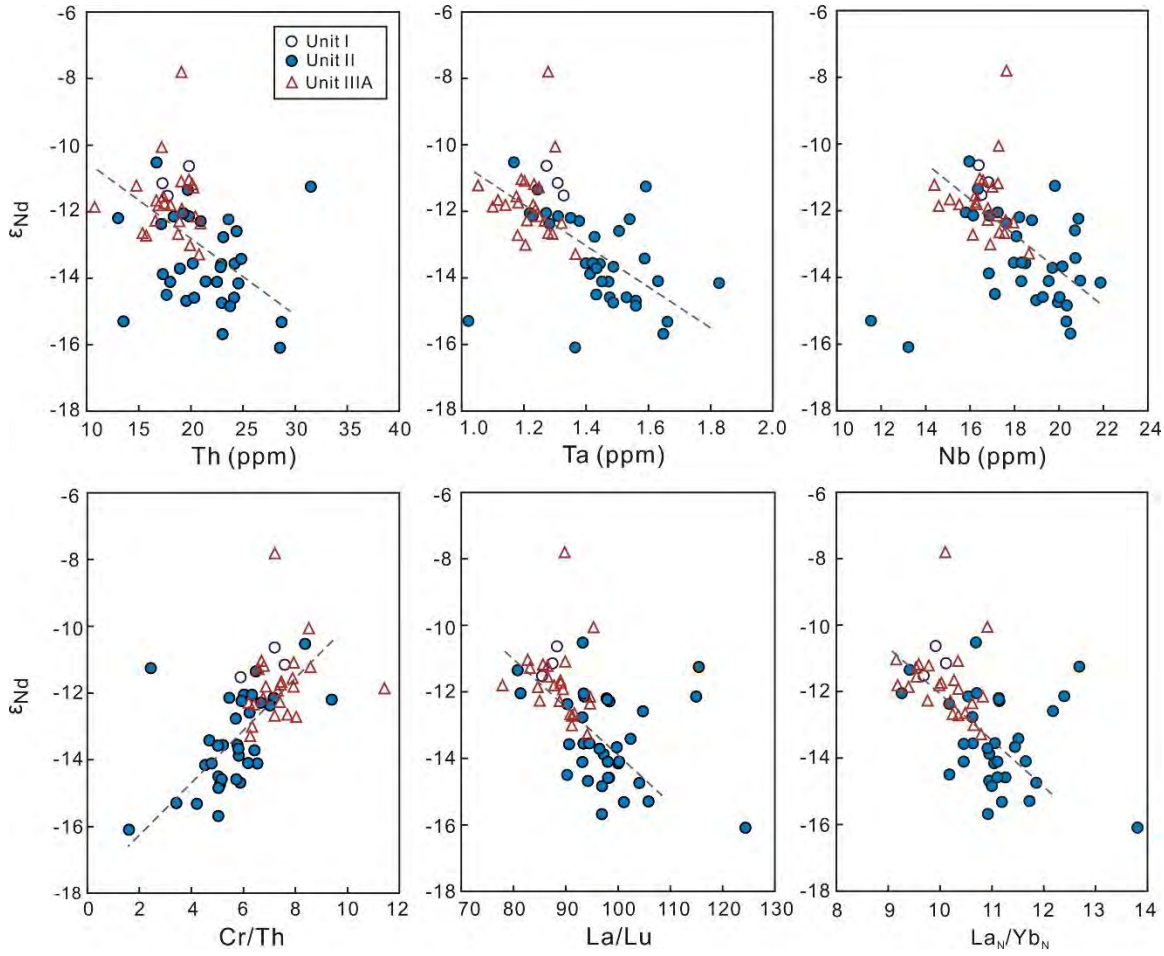

862

863 **Fig. 6**

864

865

866

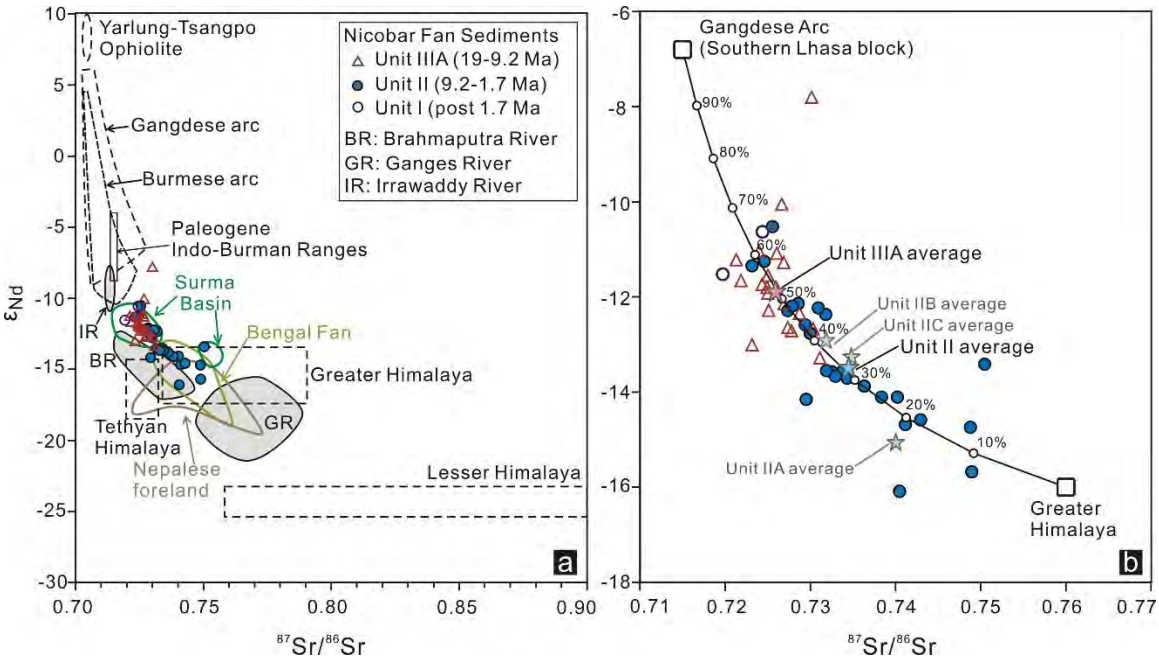

867

868 **Fig. 7**

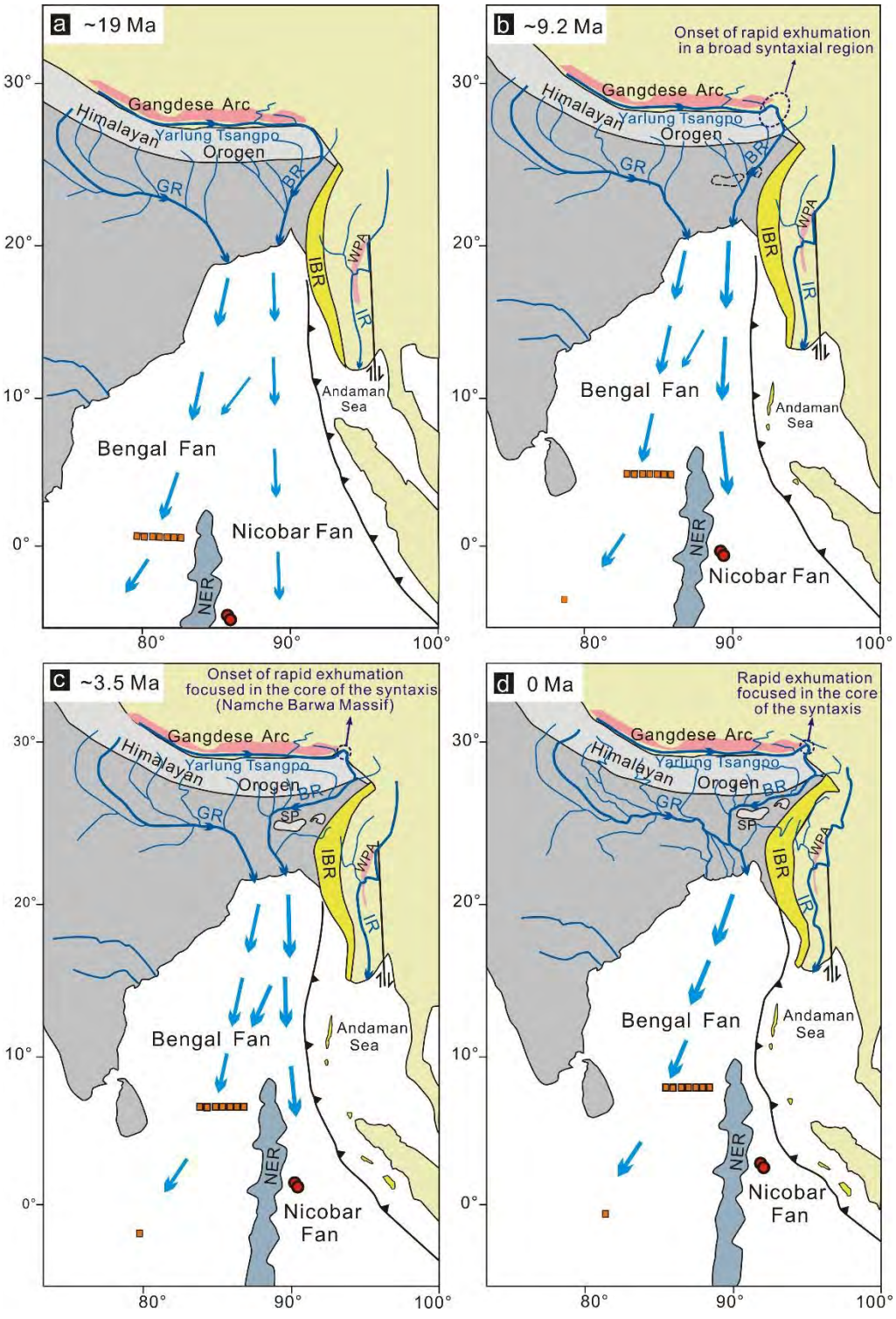

869

870 **Fig. 8**

871

Figure 1

Click here to download Figure: Figure 1.pdf

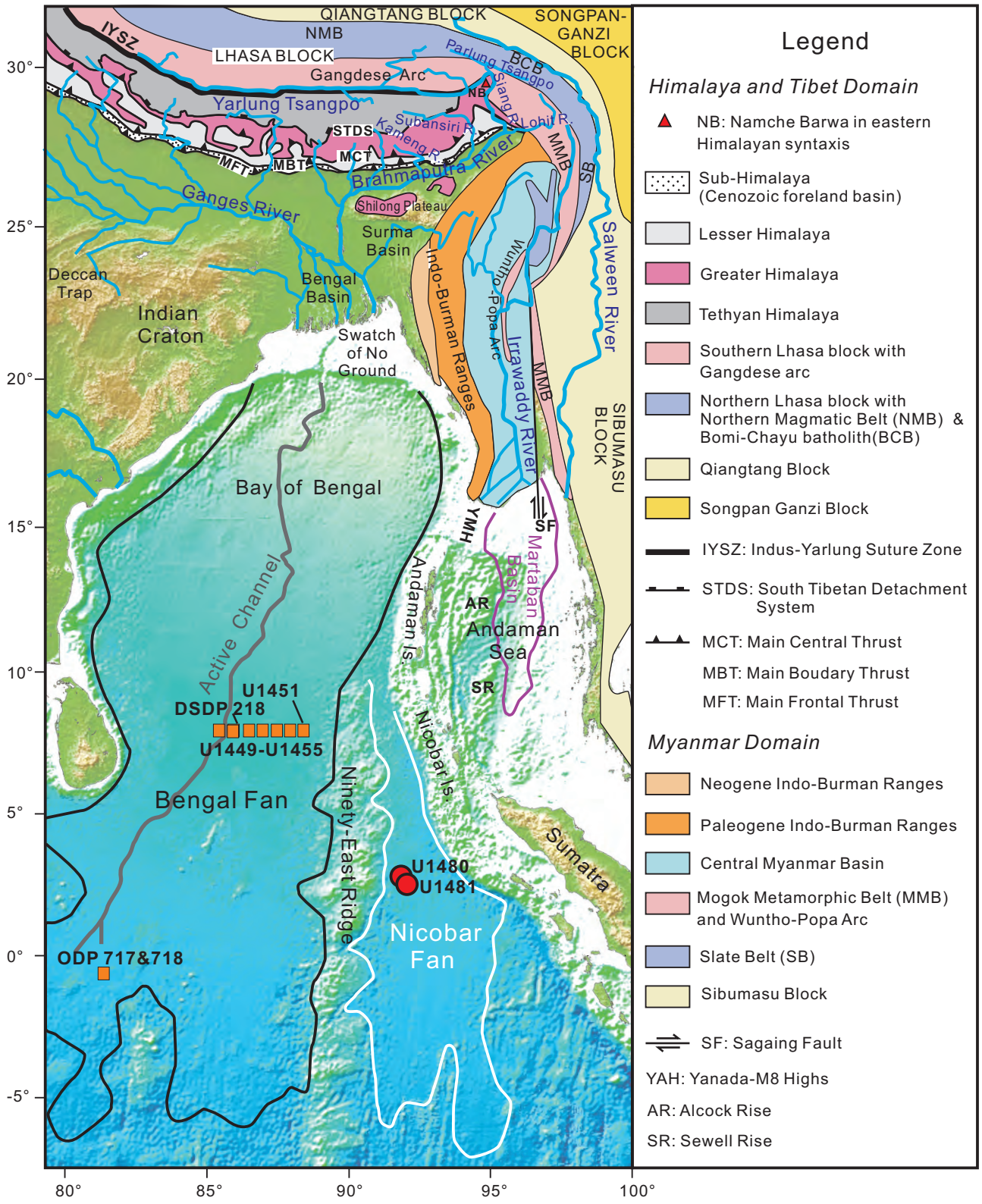

Figure 2

Click here to download Figure: Figure 2.pdf

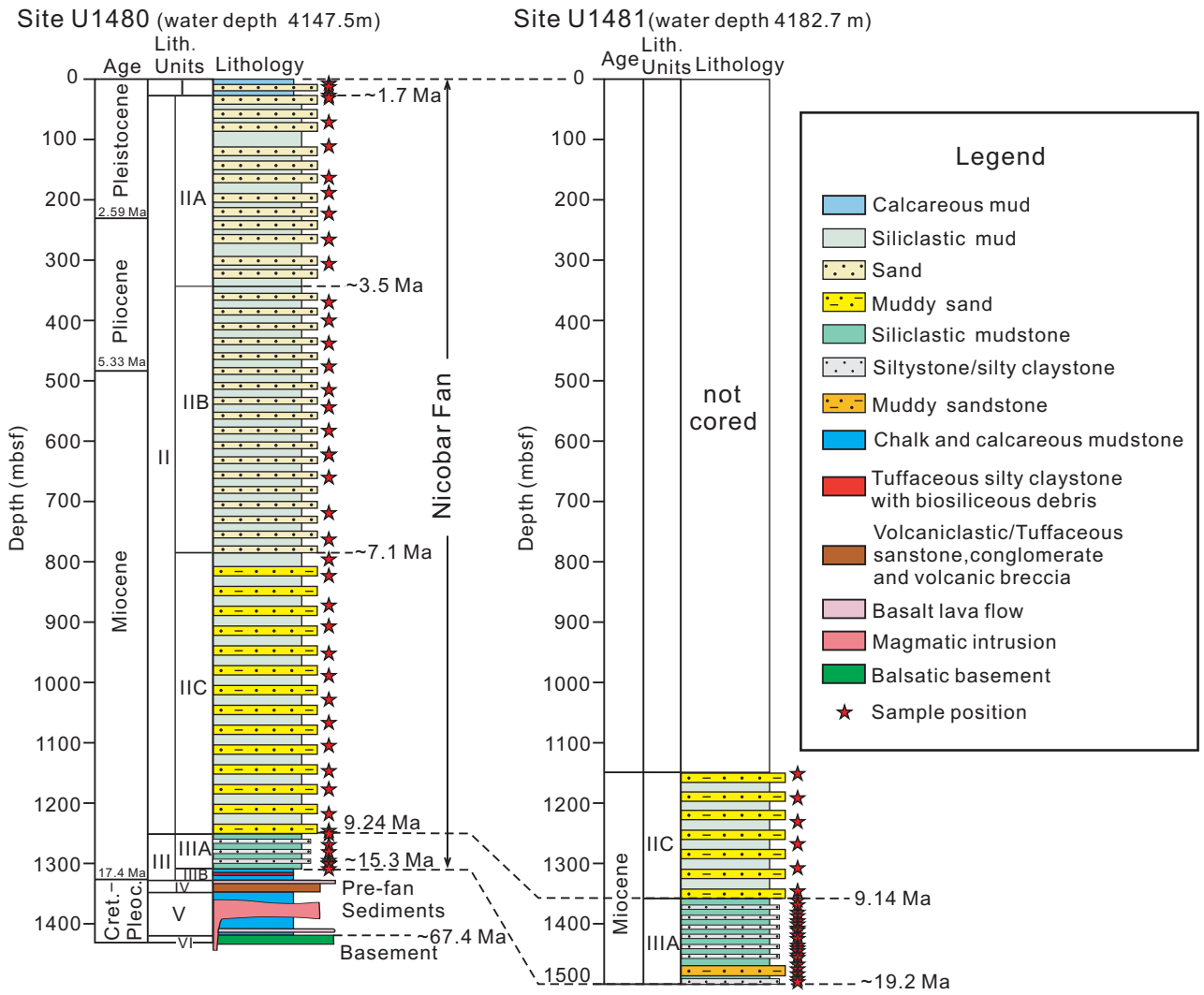

Figure 3

Click here to download Figure: Figure 3.pdf

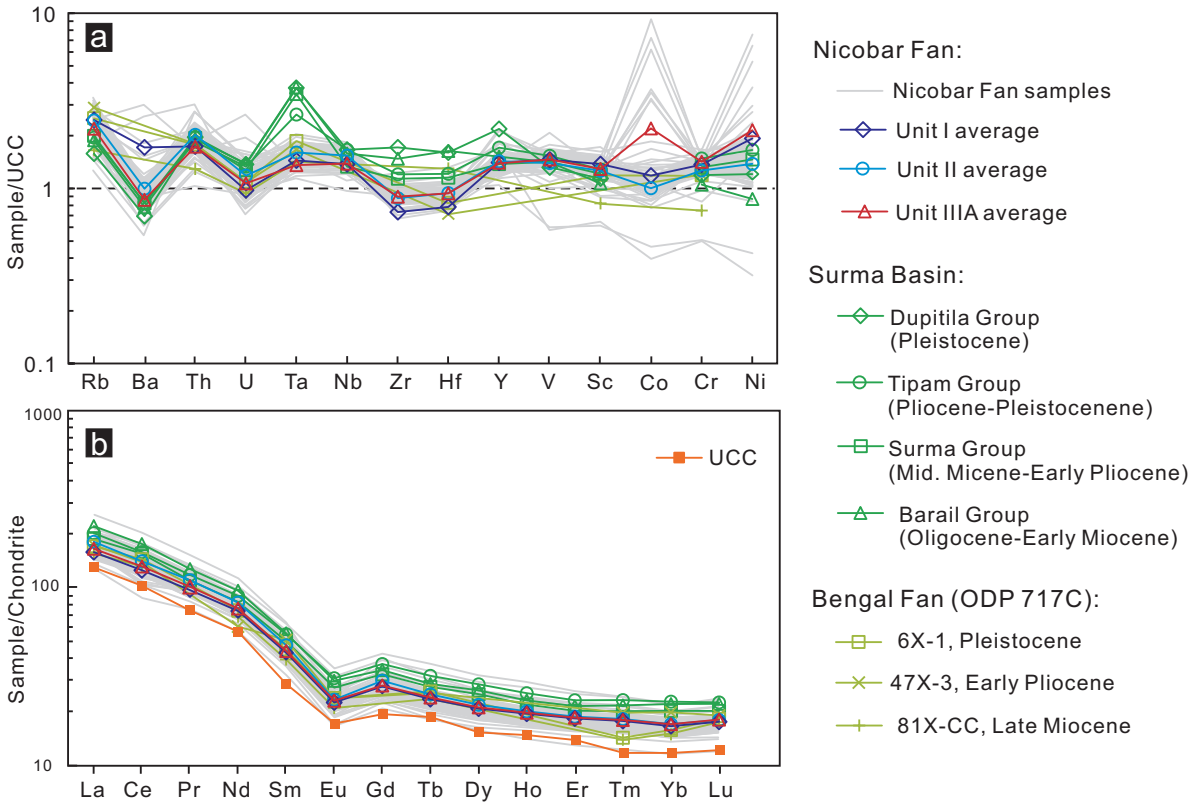

Figure 4

Click here to download Figure: Figure 4.pdf

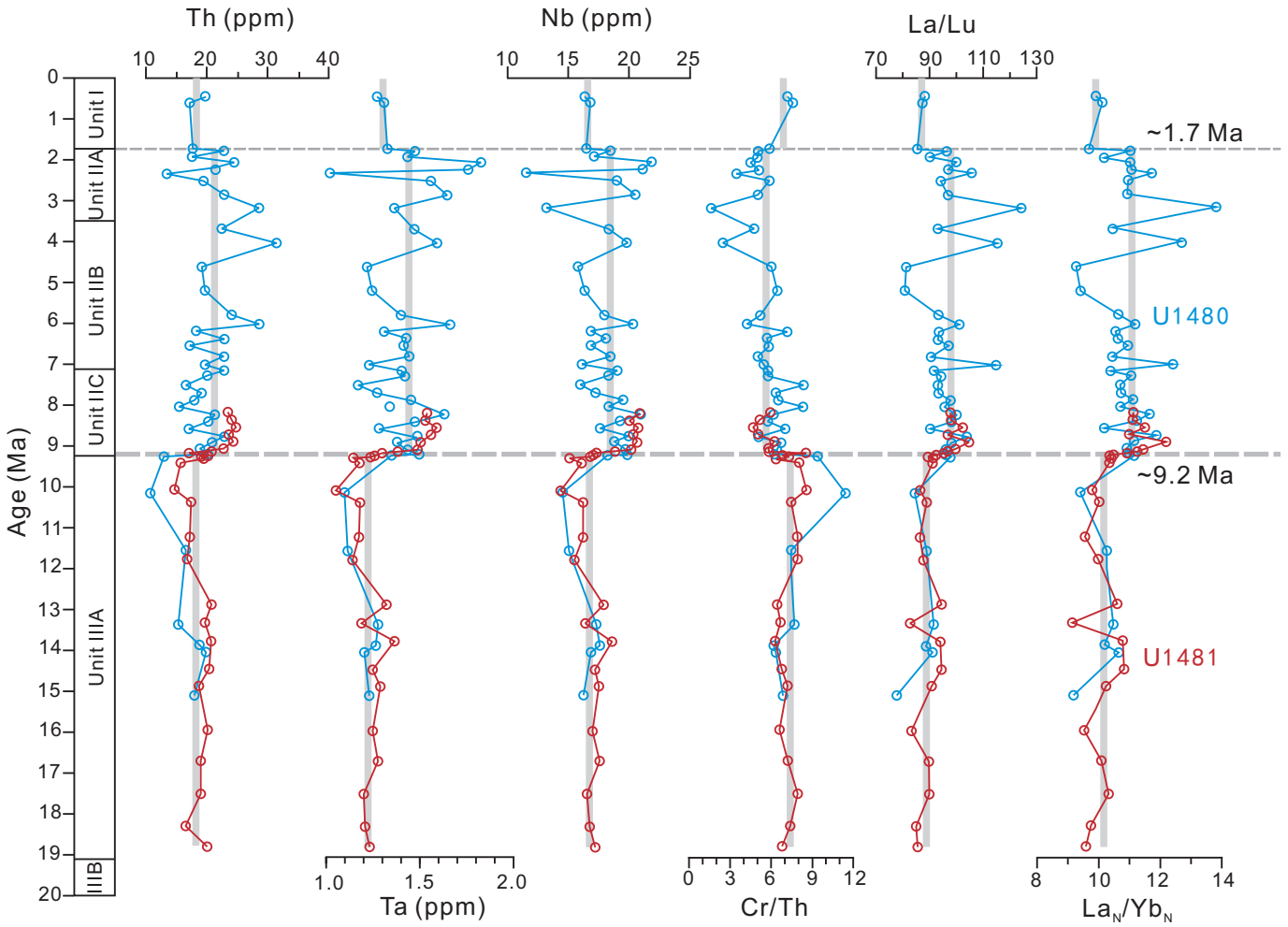

Figure 5

Click here to download Figure: Figure 5.pdf

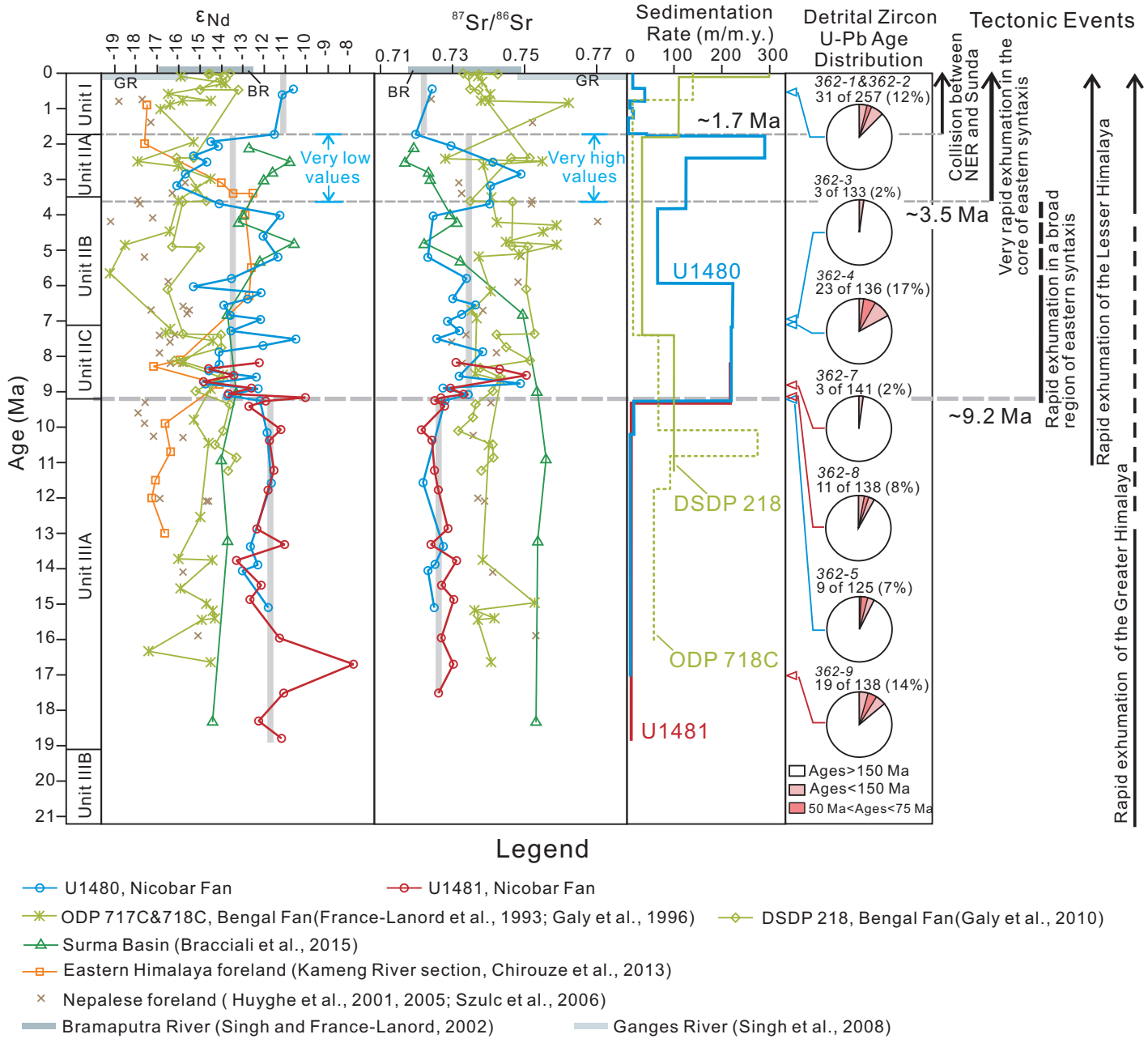

Figure 6

Click here to download Figure: Figure 6.pdf

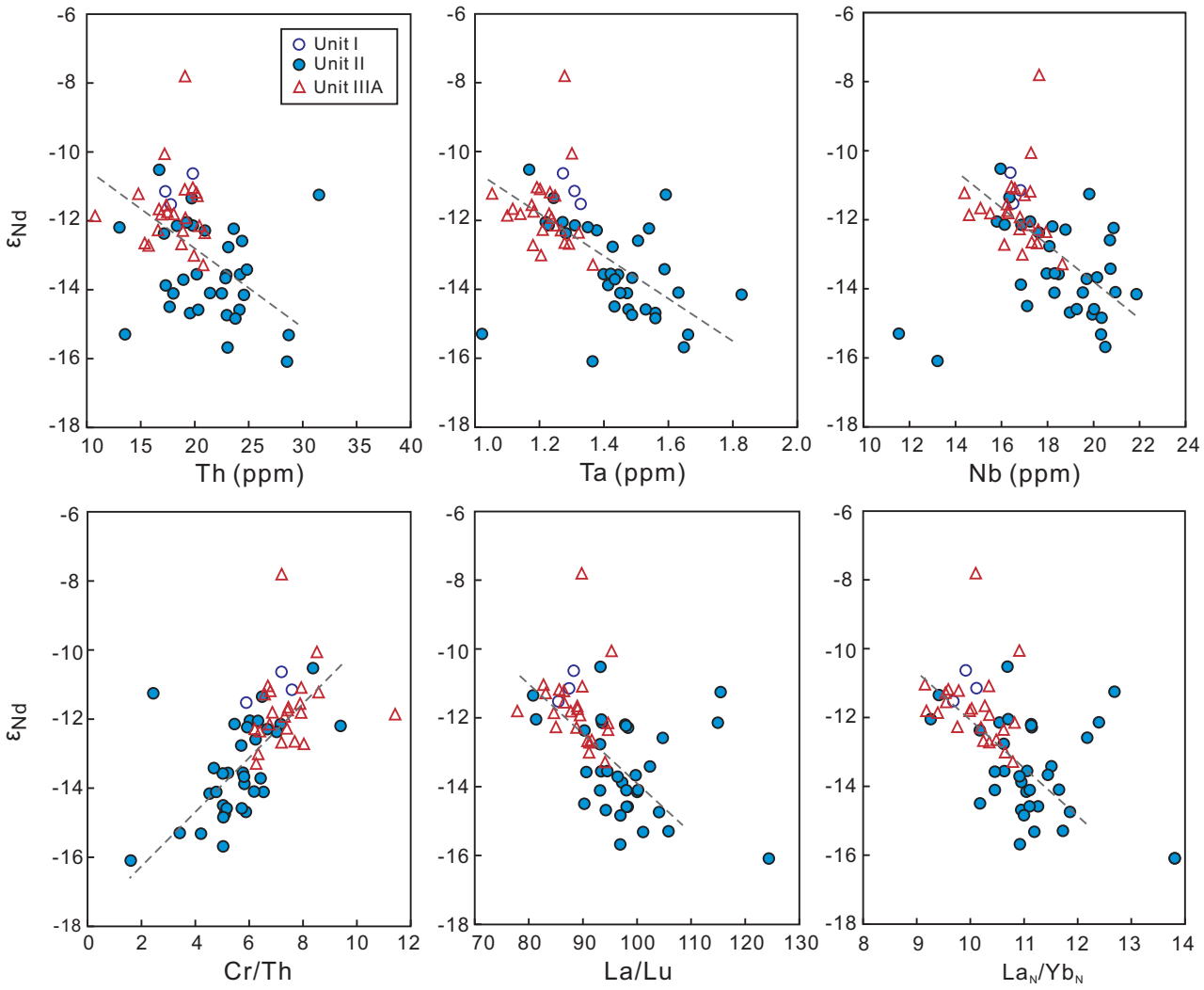

Figure 7

Click here to download Figure: Figure 7.pdf

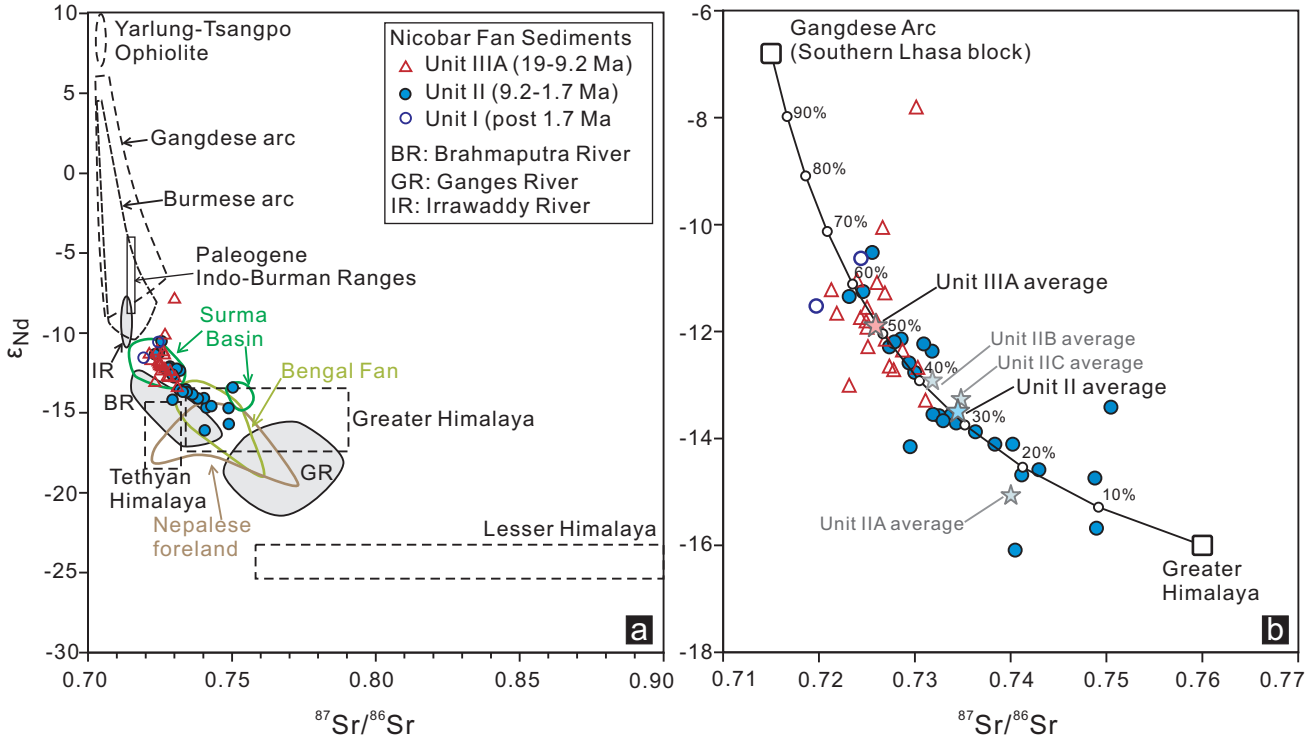

Figure 8

Click here to download Figure: Figure 8.pdf